A | T | C | T
Application and Theory of Computer Technology

Article

Computer analysis of molten steel flow and application to design of nozzles for continuous casting system

Arito Mizobe [1,*], Jouji Kurisu [2] and Masanori Ueki [3]

[1] Krosaki Harima Corporation; mizobe.fxm.arito@krosaki.co.jp
[2] Krosaki Harima Corporation; kurisu.9v7.jouji@krosaki.co.jp
[3] Ueki Professional Engineer's Office; pe35733@kanto.me
* Correspondence: mizobe.fxm.arito@krosaki.co.jp; Tel.: +81-93-622-7230

Received: 10-March-2018; Accepted: 10-May-2018; Published: 17-May-2018

Abstract: In steel continuous casting system, nozzles have an important role on the flow rate control of the molten steel and the elimination of the inclusions etc. Based on the fundamental principle of hydrodynamics, the optimal nozzle bore profile was determined for both tundish (TD) upper nozzle and submerged entry nozzle (SEN) with aiming to suppress the turbulence with high kinetic energy generated in the flow of the molten steel. A simulation by flow analysis using computational fluid dynamics (CFD) and a water model experiment were performed and clarified that the turbulence with high kinetic energy could be minimized in the nozzles with newly devised inner bore profile. The actual nozzle devised was manufactured and tested in the steel works with satisfying results. The adhesion of the alumina inclusions to the both nozzles is reduced by lowering the turbulent kinetic energy since the energy loss is minimized at the part. Both stability in the operation and quality of the steels have been brought by the present development.

Keywords: Computational fluid dynamics (CFD), Continuous casting (CC) system, Molten steel flow, Tundish (TD) upper nozzle, Inner bore shape, Flow analysis, Submerged entry nozzle (SEN), Turbulent flow

1. Introduction

Computational fluid dynamics (CFD) has been applied in recent decades since year of around 2000, for the analysis of molten steel flow and inclusion behavior in continuous casting (CC) system as one of the most useful approaches. Since the CC is very high temperature process dealing liquid state of steel at around 1550 ºC with certain difficulty to conduct experiments at such temperatures the CFD method is used effectively to simulate the behavior. Using the CFD, the authors [1,2] have presented papers on methodology of the designing nozzles for use in the CC system. Recently, Hernandez et al. have also presented [3,4] new geometrical design for submerged entry nozzle for slab CC of the molten steel with higher performance compared to that of a conventional cylindrical nozzle using the CFD software. Applying a hybrid turbulent model, Mohammadi-Ghaleni et al. [5] have presented a paper on a simulative study of molten steel flow patterns and particle-wall interactions inside the slide gate (SG) nozzle based on the CFD. Although there are several approaches carried out by groups except for them described above to analyze the molten steel flow using the CFD [6-11] and some cases together with a water model experiment [12-14], none of approaches have derived directly optimum geometry of the key devices such as nozzles on the CC system to suppress the turbulence of the flow. As the key devices, the authors would like to close the tundish (TD) upper nozzle and the submerged entry nozzle (SEN) in the present investigation.

As for the TD nozzle, the concept which serves as the foundation about the design of the inner bore profile of the nozzle for suppressing the energy loss due to turbulence in the molten steel flow to the minimum has been proposed through a different method from the "non-swirl nozzle" by Halliday [15] at 1959. The design concept was then examined its effectiveness through the flow analysis by the CFD and the water model experiment. Furthermore, the upper nozzle which has the optimum bore shape determined in the experiment based on the results examined through analysis and the experiment is used in the actual CC machine, and the adhesion-proof improvement effect was confirmed not only in the bore surface of the upper nozzle but in the inner surface of the SEN installed in the lower stream side.

Through the TD upper nozzle, molten steel is poured into mould finally from the ejection ports located in the lower position of the SEN via flow rate controlling mechanisms such as SG and stopper head. In the case of slab casting, the SEN is designed generally to molten steel ejects almost horizontally despite of slight inclination by inhibiting molten steel flow in vertical downward direction in the SEN. Shape of cross section of the ejection ports are generally rectangular or round (type), and width and height of the port are kept constant linearly from inner to outer diameter wall toward molten steel flow. To avoid abrupt velocity change in the inner diameter side of ejection port, modification of the geometry to make "corner cut" at the upper part of the SEN inner wall side which is so-called double taper port (DTP) is performed occasionally. However, adapting the geometry described above in the SEN, most of the molten steel flow out only from the lower side in outlet of ejection port, resulting in considerably higher velocity difference in upper and lower directions in the molten steel flow in the mould. Thus, since the higher side of the velocity tends to increase easily the maximum port velocity (MPV) in significant extent, in some case back flow of the molten steel will happen at upper part of outlet of ejection port for the worst case. The high extent of the MPV derives increase in not only flow velocity in the mould totally but also inhomogeneity of the molten steel flow by increasing velocity to collide to the edge part of the mould. For stabilizing the molten steel flow in the mould, homogenization of the ejection flow velocity and decrease in the MPV must be required. Theoretical background for geometrical design to suppress the flow energy loss in the course from inlet to outlet of ejection port of the SEN and minimize the MPV are explained at first. In the case of ejection port geometry derived from the theory mentioned above it is confirmed that the molten steel flow velocity in the outlet of ejection port becomes extremely homogeneous and facilitates to decrease the MPV minimum limit by means of both fluid analysis using the CFD and the water model experiment. Furthermore, the adhesion of the Al_2O_3 inclusions in the molten steel to the part of ejection port and the erosion wear of the nozzle material by turbulent flow are inhibited by decreasing frequency of the collision of the inclusions to the surface of nozzle due to minimization of the energy loss at ejection port with suppressing the turbulent energy to the minimum limit. Namely, application of the new geometry SEN to the CC operation is highly expected to contribute to process innovation of the steel production in terms of the increase in stability of the operation itself as well as quality of the products through minimizing the MPV of the molten steel flow and improving the adhesive and abrasive properties of the SEN.

2. Characteristics of the Molten Steel Flow

The molten steel flow in the nozzle (circular pipe) in this simulation model are considered with comparison of the flow of water from a viewpoint of the Reynolds number, R_e. That is, R_e is expressed with the following Eq. (1), when the average flow velocity is set to U and the diameter of the nozzle, d (=2R) and coefficient of kinematic viscosity of a fluid is set to ν.

$$R_e = Ud / \nu, \tag{1}$$

From experimental value of the coefficient-of-viscosity [16] of 5.35-5.76cP (5.35-5.76x10^{-3}Pa·s) at 1500-1650ºC for Fe-0.18%C steel, the approximate value of the ν as 0.84-0.76x10^{-6}m²/s was acquired using density value [16] of 7.0-6.8g/cm³ in this temperature region for the similar composition of the steel (0.35%C). Based on this, the approximate values of the Reynolds number calculated using the Eq. (1) are shown in Table 1 for each of low- and high-flow velocity conditions for the case of d=70mm. It turns out that the Reynolds number of molten steel is almost the same as value of the water for each condition.

Table 1. Calculated Reynolds number (×10^3) of the molten steel and water for two flow velocity conditions.

Flow velocity \ Material / Temp.		Molten steel at 1500 ºC	Molten steel at 1650 ºC	Water at 25 ºC
1.76ℓ/s	(0.46 m/s)	38	42	32
4.485ℓ /s	(1.17 m/s)	97	107	82

Generally, in the flow in circular pipe, the behavior of the flow changes by R_e=2320, and at the R_e larger than this value, pressure loss increases in proportion to the approximately 2nd power of the average flow velocity. And the flow of this domain is called "turbulence", a three-dimensional swirl exists in the flow in turbulence, and it is divided and/or unified repeatedly, and it exhibits time to time change locally [17], and it is possible to consider that such disorder in the flow brings about the increase in loss. That is, the flow in the nozzle dealt with the present investigation is the turbulence region whose Reynolds number is all in the range of 32-107x10^3, for both molten steel and water as shown in Table 1.

On the other hand, in the "laminar-flow" region whose Reynolds number is 2320 or less, the velocity distribution in the circular pipe shows the shape of the parabola (the 1/2 power rule), as shown in Figure 1(a), but if it becomes turbulence region, as similarly shown in the figure, the flow velocity in the pipe center part falls, and, generally becoming flat velocity distribution (the 1/7 power rule) is known [17].

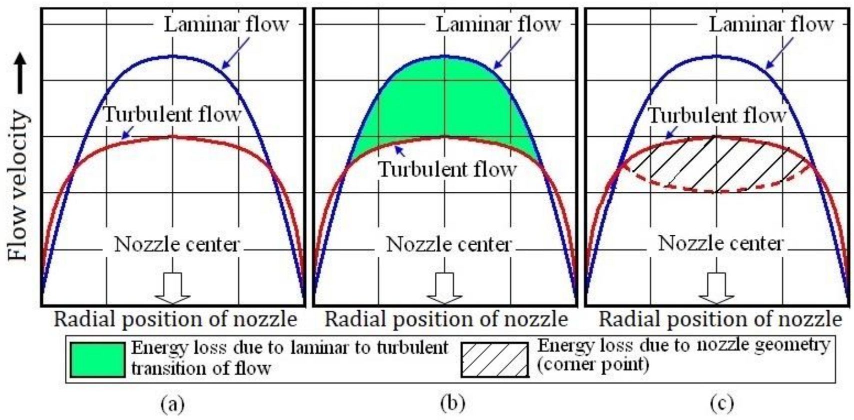

Figure 1. Schematic illustration of difference in flow velocity distribution of the laminar and the turbulent flow (a), concept of energy loss due to flow transition from laminar to turbulent (b) and the energy loss due to nozzle geometry in the turbulent flow (c).

3. Molten Steel Flow to be essentially controlled in the CC System

CC is defined as teeming of a liquid metal in a short mould with a false bottom through which partially solidified ingot is continuously withdrawn at the same rate at which metal is poured in the mould. Steel continuous casting is a process in which liquid steel is continuously solidified into a strand of metal. Depending on the dimensions of the strand, these semi-finished products are called slabs (flat products, i.e. plate, sheet, coils), blooms (long products, i.e. bars, beams) and billets (long products, i.e. bars, channels, wires). The process was invented in the 1950s to improve the productivity of steel manufacturing. Previously only ingot casting was available which still has its benefits and advantages but does not always meet the productivity demands. Since then, CC has been developed further to improve on yield, quality and cost efficiency. The advantages of CC over ingot casting are better quality of the cast product, no need to have slabbing/blooming or billet mill as required when ingot casting is used, higher extent of automation is possible, width of the slab can be adjusted with the downstream strip mill, less segregation in continuously cast products and hot direct charging of the cast product for rolling is possible which leads to energy saving.

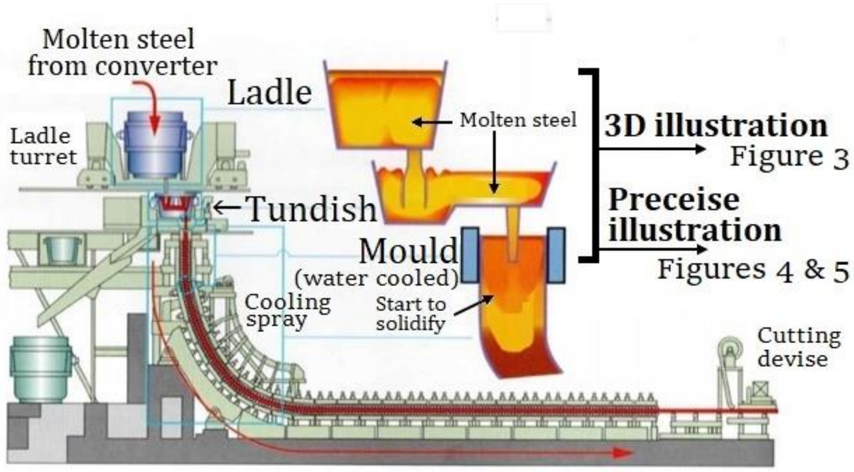

Figure 2. Arrangement of ladle, TD and mould in a curved CC system [18].

Arrangement of each equipment and flow of the molten steel in the CC system is schematically shown in **Figure 2**. The system is composed of various parts such as ladle turret, ladle, TD, mould, withdrawal rolls, cooling spray, cutting device, the auxiliary electrical/mechanical gears to assist run the machine smoothly etc.

The molten steel is supplied to the continuous caster from the converter. The ladle is usually delivered by crane and positioned into a ladle turret, which subsequently rotates the ladle into the casting position. A SG in the bottom of the ladle is opened to allow the molten steel to flow through a protective shroud into a TD, a vessel that acts as a buffer between the ladle and the mould. As the TD fills, stopper rods are raised to allow the casting of steel into a set of water-cooled copper moulds underneath the TD as shown in Figure 3 [18] as a 3-D illustration. Solidification begins at the mould walls and the steel is withdrawn from the mould by a dummy bar. Throughout the entire casting process, the mould oscillates vertically to separate the solidified steel from the copper mould. The strand is withdrawn from the mould by a set of rolls which guide the steel through an arc until the strand is horizontal. The rolls have to be positioned close enough together to avoid bulging or breaking of the thin shell. As the steel leaves the mould, it has only a thin solidified shell which needs further cooling to complete the solidification process. This is achieved in the so-called secondary cooling zone, in which a system of water sprays situated between the rolls are used to deliver a fine water mist onto the steel surface. At this point, the steel, solidified shell and liquid center, is called the strand. After the strand has been straightened and has fully solidified, it is torch-cut to pre-determined product lengths. These are either discharged to a storage area or to the hot rolling mill.

 Appl. Theory Comput. Technol. **2017**, 2, 4; doi: 10.22496/atct.v2i4.115

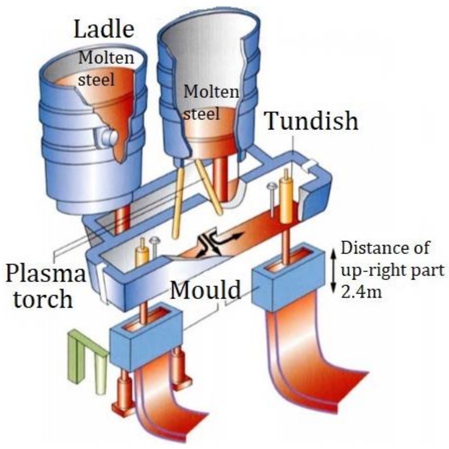

Figure 3. 3-D illustration of an example of major parts of the CC system [18].

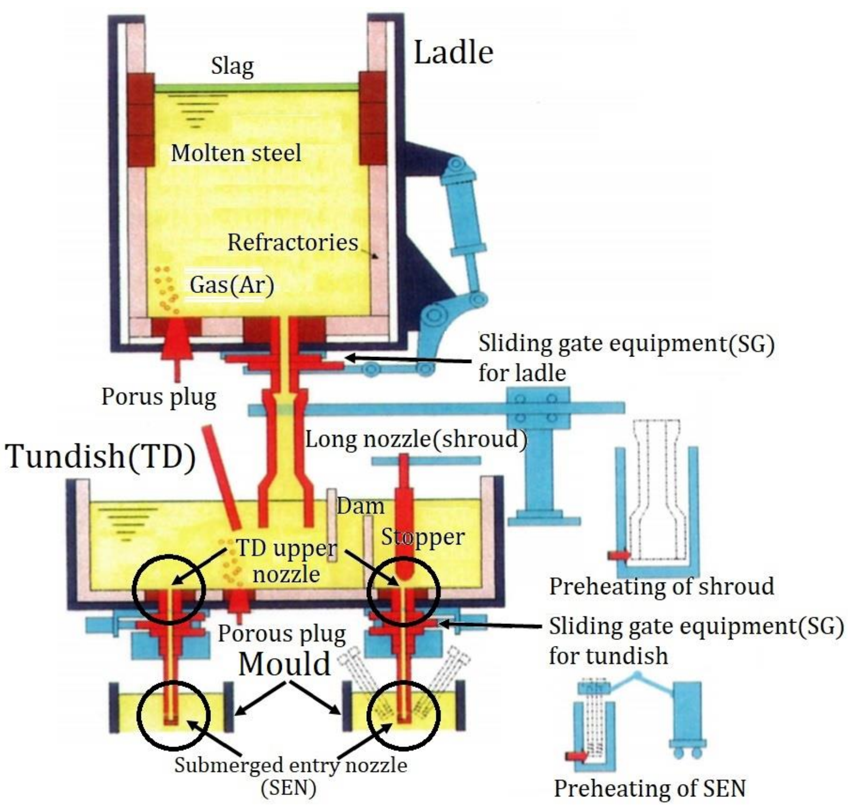

Figure 4. Precise description of major parts of CC system dealing the molten steel [19].

 Appl. Theory Comput. Technol. **2017**, 2, 4; doi: 10.22496/atct.v2i4.115

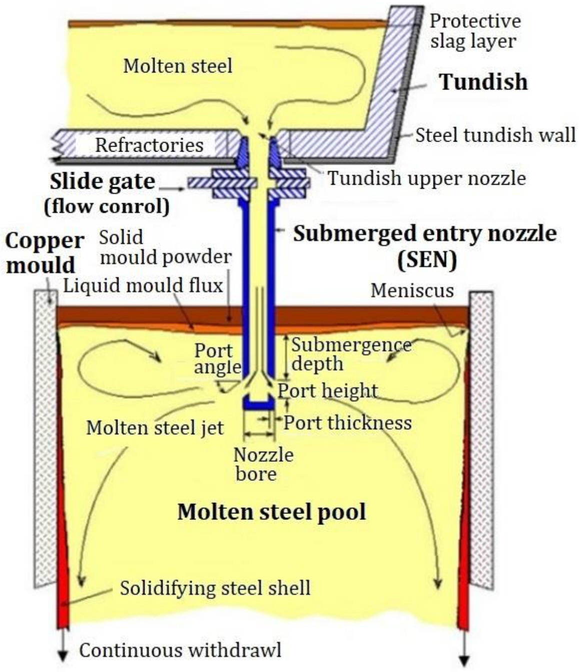

Figure 5. Schematic detail of TD, SEN and mould in the CC system [20].

Detail of the movement of the molten steel from the ladle to the mould via TD is shown in Figure 4 [19] and the circled positions in the figure are essential parts to be controlled the molten steel flow. Then, in Figure 5 [20], one of the pair in left and right-hand sides of circled part in the Figure 4 is magnified to show the molten steel flow in more detail. During CC processes impurities like deoxidation products in the melt deposit at the walls of the TD nozzle and the stopper. This phenomenon, termed clogging, causes obstruction of the flow and deteriorate the quality of the steel product. A detailed knowledge of the flow pattern within the TD nozzle-stopper region is very important for the design of appropriate nozzle and stopper geometries. By means of a numerical simulation the important influence of turbulence on the velocity field of the molten steel in the nozzle region could be demonstrated that most of the particles close to the walls are deposited in case of high turbulence. A new design for the nozzles proposed in the present investigation may reduce turbulence, prevent recirculation and permit a weaker lateral particle transport.

4. Design of Nozzles for passing Molten Steel based on Flow Analysis

4. 1. TD Upper Nozzle

Adhesion of Al_2O_3 system inclusion in molten steel occurs in the inner bore of pouring upper nozzle installed in the CC TD. The cross-sectional area of the inner bore will be reduced when adhesion occurred, and if the adhesion increased further, the nozzle clogging will be caused, and resulting in the interruption of the operation. Al_2O_3 system or Al_2O_3-C system refractories are mainly used as the upper nozzle material. Although there is a possibility that adhesion-proof will be slightly improved by difference in the materials selected, it has not yet resulted in fundamental solution. Moreover, although there is also technology which gives adhesion-proof by blowing inert gas by penetration hole installation or application of the gas permeable porous material for the nozzle and making small contact probability on the surface of refractories of the inclusion in the molten steel, however, as a result, sufficient improvement of adhesion-proof just by such way is not obtained because of difficulty to cover the whole refractories surface by blowing-in gas. As for the shape of the nozzle, there have been no report other than so called non-swirl nozzle by Halliday of the 1950s [15].

4.1.1. Underlying concept on flow in the TD upper nozzle

In the molten steel flow of the bore in a nozzle, Figure 6 explains the underlying concept of the bore shape determination in the nozzle as conditions for minimizing the energy loss by turbulence. The flow velocity of the molten steel which flows through the bore in the nozzle, V, is obtained by transforming the potential energy determined by the height (depth) from the meniscus H_r of TD, into the kinetic energy. From an energy-conservation-law [21], if static pressure of the system is set to P, molten steel density will be set to ρ, and acceleration due to gravity will be set to g, the following Eq. (2) (Bernouilli equation) will be hold.

$$\rho V^2/2+\rho g\, H_r + P = Const., \tag{2}$$

If it is applied to at the molten steel surface (meniscus) (subscript '0') and the outlet of the nozzle (subscript '1'),

$$\rho V_0{}^2/2+\rho g\, H_r+P_0 = \rho V_1{}^2/2+P_1, \tag{3}$$

It can be regarded as $V_0 = 0$, because the area of the meniscus is so large compared to that of the nozzle bore. The pressure at meniscus and the pressure of the outlet are also considered as the atmospheric pressure, it is set to $P_0 = P_1 = 0$ (gauge pressure). Eq. (3), therefore, can be modified as follows,

$$V = (2gH_r)^{1/2}, \tag{4}$$

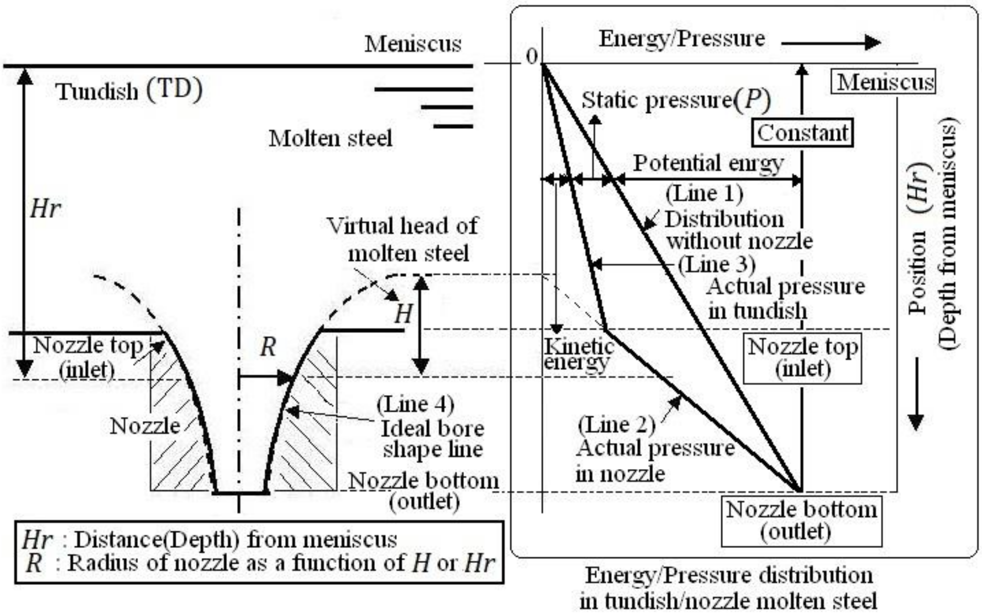

Figure 6. Schematic illustration of the vertical section of TD and its upper nozzle to explain a fundamental concept for suppression of intensified kinetic energy for the turbulent flow in the nozzle based on the pressure distribution in the TD shown in the right-hand figure.

Here, the 1st term of the left side of the Eq. (2) is the kinetic energy, and the 2nd term of the left side is the potential energy. Then, in Figure 6, in whole structure including a nozzle, the domain on the right side of Line1 in the right-hand figure can show potential energy in the depth direction of the TD, i.e., the bore height direction in the nozzle. If the kinetic energy can be expressed in linear function (straight line) like Line1, P will become a constant, as for it, all the energy distribution will be stabilized, and it will be thought that it is ideal. However, since the TD is installed for stabilization of the molten steel flow and for inclusion surfacing in molten steel in the CC operation, it has big enough capacity. Therefore, as mentioned above, in the TD the flow velocity of the molten steel will be able to be considered as zero except for the very vicinity of the nozzle inlet. Thus, the conversion to kinetic energy from potential energy is generated only inside the nozzle. The kinetic energy change inside the nozzle is large as shown in Line2 in the right-hand figure, but within the TD until the molten steel flow reaches there, namely the inlet of nozzle, as shown in Line3 in the right-hand figure, the kinetic energy change is comparatively small. In addition, the domain of the left side of the Line1 and the right side of the Line2 or Line3 in the figure is equivalent to the above mentioned static pressure, P. That is, when the molten steel reaches the nozzle inlet part, it means that rapid energy conversion takes place. Therefore, if this energy (pressure) change by the bore in the nozzle including the nozzle inlet can be made small as much as possible, overall, energy loss will become small and will become possible suppressing the energy loss by the turbulence in the molten steel flow in the nozzle bore to the minimum. Thus, generation and growth of the inclusion in the molten steel are confined, and probability that the inclusion will contact to the nozzle bore surface can be made small, and it is thought that it becomes possible as the result to decrease the adhesion of the inclusion to the refractories.

It is possible to consider that the molten steel flow through the upper nozzle of the TD is similar problem of general hydrodynamics [22] on the "energy loss in the fluid flow through the pipe in which section reduces suddenly". It was known on experience that the energy loss is small in the pipe inlet in this case for the diameter reducing pipe (nozzle) which gave a certain curvature like the shape of trumpet. However, in the Figure 6, the trial which determines the shape of the curve shown by Line4 strictly is not yet made so far.

According to the following methods, the shape of this curve (correctly curved surface) will be determined here. If the amount of flow is set to Q and the flow velocity V and the bore cross-sectional area in the nozzle are set to A in the nozzle bore, the following relation will be hold from the continuity of fluid [21] in every height position of the nozzle.

$$Q = VA = Const., \tag{5}$$

Here, in practice, since the molten steel flow Q is controlled (restricted) by the SG (it does not appear in the Figure 6) installed in the connection to the nozzle bottom, considering the molten steel head H of imagination, the Eq. (4) is expressed as follows.

$$V = (2gH)^{1/2}, \tag{6}$$

And from the radius of the nozzle, R, since $A = \pi R^2$, the Eq. (5) becomes to the following relation.

$$(2gH)^{1/2}\pi R^2 = Const., \tag{7}$$

Finally, the relation of the following formula is hold in between the nozzle radius R and the virtual molten steel head (height) H.

$$R \propto H^{-1/4}, \tag{8}$$

That is, as for the formula (8), it is a solution obtained for the first time for the determination of the curve shown as Line4 in the Figure 6 which is a curve expressing the bore profile in the nozzle which makes energy loss the minimum, and it is the 4th curve (Biquadratic). Furthermore, since the relation of $V^2 \propto H$ holds from the Eq. (6), that is, kinetic energy (V^2) and height (depth) H have a straight line relation. Since the static pressure P which is the difference from all the energies has straight line relation with the height (depth) H, the Line2 of the right-hand figure in the Figure 6 can be expressed in a straight line (see also bottom figure in the Figure 9(b)).

4.1.2. Flow analysis for the TD upper nozzle

Calculation was conducted with about 100,000 elements using the Fluent6.3.26 (finite volume method) system software. Analysis modeling of the molten steel flow from the TD to the upper nozzle and the SG was carried out. The coordinates set the height direction to Z_{TD}, and the lower part is the plus side, and it made the nozzle upper surface center the starting point (X_{TD}=Y_{TD}=Z_{TD}=0). Moreover, the slide direction of the SG was set to X_{TD}, and the perpendicular direction was set to Y_{TD} to Z_{TD} and X_{TD}. The molten steel surface (meniscus) in the TD was made 1m from the bottom. Calculation fluid considered it as water for a reason which was described previously, and the mass flow rate considered it as two conditions of the low- velocity 1.76 and high-velocity 4.485ℓ/s and was calculated by the *k*-omega viscosity model. As mentioned above, by making it slide, the SG is equipment which changes valve travel and performs control of the flow, and fixed valve travel with 50% was used in calculation here.

The bore shape in the nozzle taken up here can be expressed as shown in Figure 7 as the function of the radius R and the height Z_{TD}. That is, if the height position which nozzle height is 230mm and the distance from the upper end (inlet) of the nozzle to the lower part is set to Z_{TD}, Shape① has the basic profile used for the pouring nozzle (TD upper nozzle) until now, in which the nozzle outlet radius is 35mm (70mm in diameter), and the radius from the outlet to 50mm above the height direction is 35mm. And in the section, the linear taper was formed from the height position (Z_{TD}= 180mm) to the nozzle top end (Z_{TD}= 0mm), and the radius in the nozzle upper most plane is 70mm, and the curvature (radius of curvature of 295mm) was given in the corner part to avoid the rapid change at Z_{TD}= 180mm position. Shape② is the 4th curvilinear shape previously shown by the formula (8) and Line4 in the Figure 6, and the outlet 35mm in radius, and inlet 70mm in radius presupposed that it is the same as that of Shape①.

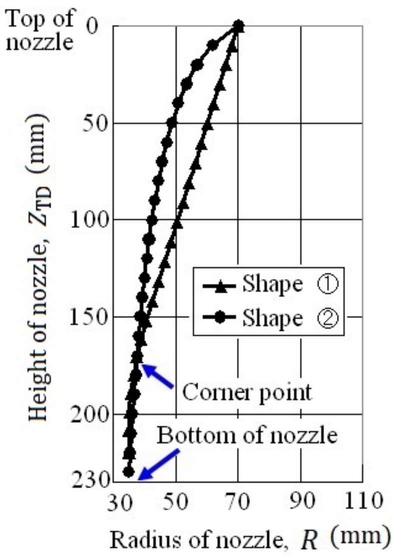

Figure 7. Representations of two nozzle bore shapes tested in the present work as the function of the nozzle height and radius.

The flow velocity distribution and the vector diagram in the nozzle obtained by the calculation are shown in Figure 8(a) and (b), respectively. For both figures, distribution in the nozzle center section (Y_{TD}=0mm section at the time of setting the direction of SG slide to X_{TD} and setting the perpendicular direction to Y_{TD}) is shown. At Shape①, although the flow velocity change in a corner part (Z_{TD}=180mm) is remarkable, it turns out that the flow velocity is changing from the inlet gradually to outlet including the neighborhood of the SG for Shape②.

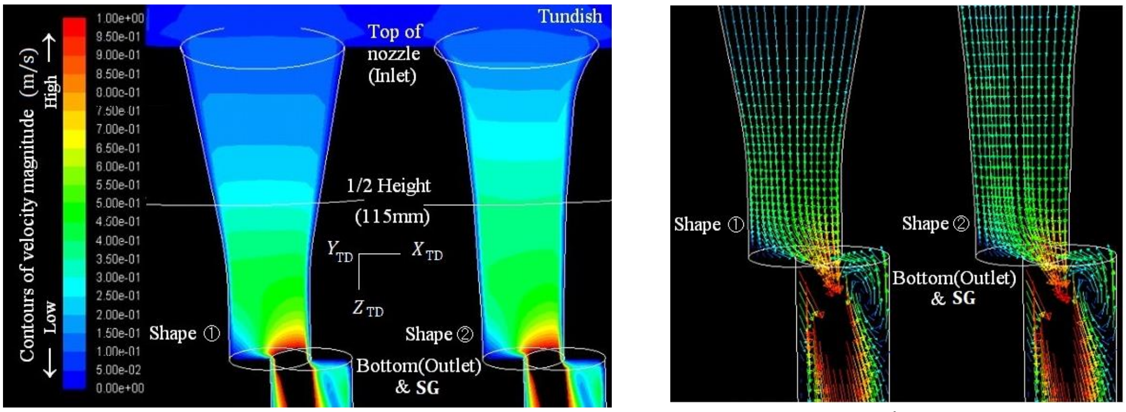

(**a**) (**b**)

Figure 8. Comparison of calculated velocity of the molten steel flow in the TD upper nozzle of Shape① and Shape② (a), and the flow velocity vectors coloured by the velocity magnitude for both shapes (b) at throughput (flow velocity) condition of 1.76ℓ/s.

In Figure 9(a) and (b), by calculation as similarly as the previous figure, Shape① and Shape② are compared respectively in both the pressure-distribution diagram in upper side and the variation of the static pressure with the nozzle (height) position in the bottom side. Here, the upper figures are the pressure distribution on the inner surface of the nozzle, and the bottom figures are the pressure distribution in the nozzle center section (Y_{TD}=0mm section). Although the pressure is declining rapidly in the corner part (Z_{TD} =180mm) for the Shape① like the velocity distribution shown in the Figure 8, it turns out that pressure is declining gradually (linearly) from the inlet to the outlet for the Shape②.

Moreover, since the flow control mechanism by the SG exists in the nozzle outlet side, the shape is largely change for both shapes at the SG open and close side, the pressure distribution is changing in the SG stroke direction (the direction of X_{TD}), comparing the bottom side figures in (a) and (b).

Next, to investigate the influence of the molten steel flow velocity, calculation on the conditions raised to 4.485ℓ/s of average flow corresponding to the actual operation was performed. The velocity-distribution diagrams for both shapes are shown in Figure 10. Shape② exhibits uniform velocity distribution, but the Shape① showed the unique radial-velocity distribution to which a high-speed region is seen in the corner part (Z_{TD}= 180mm) by the portion near the nozzle wall, and a low-speed region exists in the center part, and the stability of the flow disappeared. Next, as shown previously in the Figure 1(a), the velocity distribution of the corner part for both cases was compared as shown in the Figure 11(a). In Shape②, velocity distribution is rather "flat" form peculiar to turbulence, showing the velocity distribution almost uniform from the portion near the nozzle outer wall to the center part, but in Shape①, the velocity became low in the nozzle center part and the velocity became high near the nozzle surface (position at where a radius position ± is large except for the real surface), and namely there was a considerable velocity change in the radial direction. It is, thus, thought that the area under the curve which shows velocity distribution expresses energy notionally, the energy loss by changing from laminar to turbulent flow can be shown as the area difference in the Figure 1(b). Then, the energy loss in Shape① shown here can be expressed with the slash part (a centerline is separated and only a half is illustrated) shown in Figure 11(b). That is, it is typically shown in the Figure 1(c), and the area of these slash parts can be considered as energy loss by the shape of the nozzle also in turbulence from the energy loss by the changes to turbulence from the laminar flow. Furthermore, although Figure 12 shows the calculation result of kinetic energy distribution for turbulence, in Shape①, the turbulence with high energy occurs in the nozzle central part in the height position of the corner part, and the high turbulence energy also is seen in the SG entrance part. However, in the Shape②, the high turbulence energy is not seen within the nozzle, and even in the SG entrance part, the energy is not so high, either. That is, it is thought that the existence of turbulence generating with the high kinetic energy in the upper stream affects to the downstream SG section.

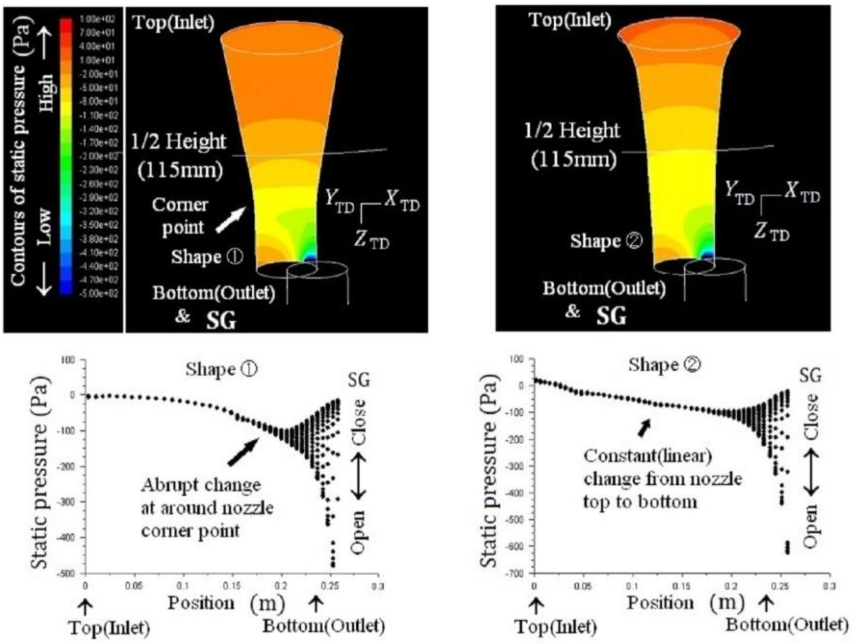

(a) (b)

Figure 9. Comparison of calculated static pressure of the molten steel flow at flow velocity of 1.76ℓ/s for the TD upper nozzle and the graphic presentation of the static pressure change with position from top to bottom of the nozzle for both Shape① and Shape② in (a) and (b), respectively.

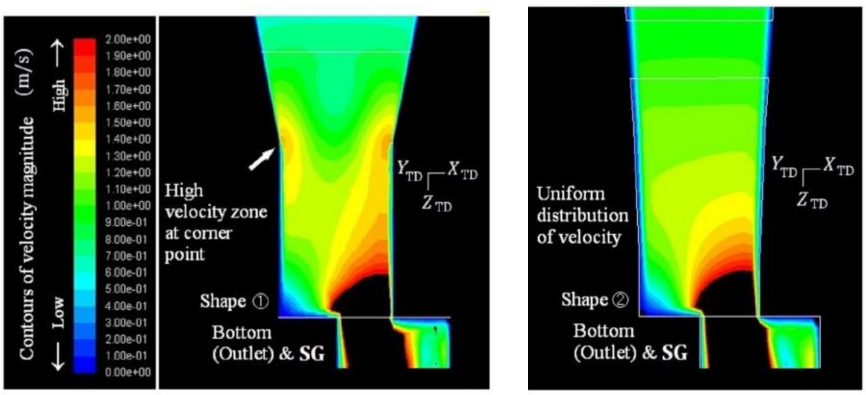

(a) (b)

Figure 10. Comparison of calculated velocity of the molten steel flow for the TD upper nozzle of Shape ① and Shape② at the higher throughput (flow velocity) condition of 4.485ℓ/s.

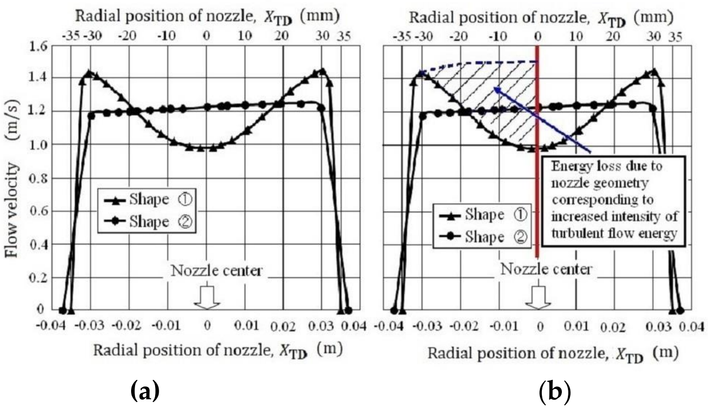

Figure 11. Comparison of the flow velocity distribution in the horizontal section of the nozzle at the height of 180mm from the top which corresponds to the corner point for nozzle of Shape① (a) and the concept of the energy loss expressed by the shaded part (1/2 of total divided by the center line) due to intensified kinetic energy of the turbulent flow (b).

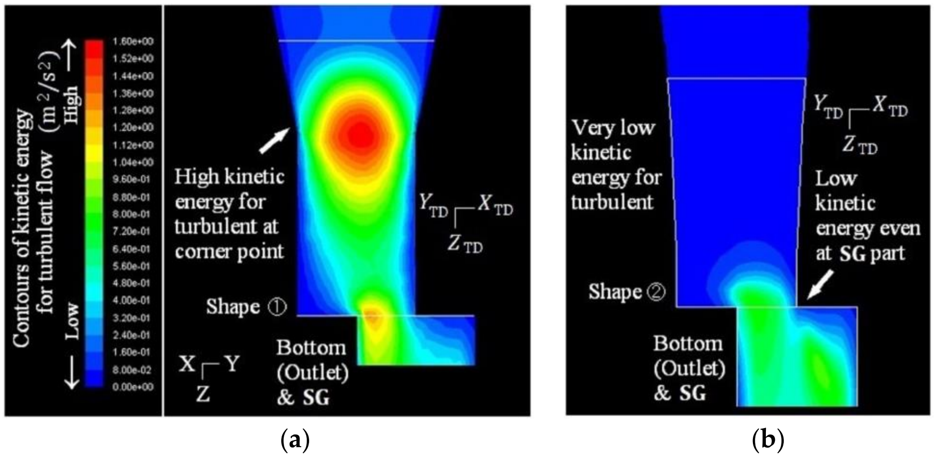

Figure 12. Comparison of calculated turbulent kinetic energy for the TD upper nozzle of Shape① and Shape② at the higher throughput (flow velocity) condition of 4.485ℓ/s.

The influence of the turbulence energy in the nozzle on the inclusion adhesion is reviewed here. Nakaoka [23] has reported that the collision frequency of inclusion particles is proportional to the 1/2 power of turbulence energy dissipation velocity based on the results [24,25] that the inclusion in the molten steel condenses by turbulence. According to these results, it is considered that growth rate of the inclusion in the bore part of the nozzle is high for Shape① with high kinetic energy of turbulence due to increased collision frequency of the inclusions inside the nozzle. Moreover, it has also described simultaneously [23] that collision frequency is proportional to the 3rd power of a particle radius, if inclusion grows, collision frequency with the nozzle surface of wall will also increase, and it will be thought that it becomes further easy to adhere. It is also suggested that when the grown-up inclusion flows for the SG plate and the SEN by the side of the lower stream, a possibility that adhesion by the part will also increase. Next, Shimasaki et al. [26,27] carried out the detailed examination about flow behavior of the molten steel, such as surfacing and sedimentation of the particles in flow with turbulence. The relative velocity of Al_2O_3 inclusion particles in the molten steel is greatly dependent on intensity of turbulence, and it is shown clearly in the portion with strong turbulence that relative velocity decreases sharply etc. And about the adhesion behavior on the surface of a nozzle Mukai et al. [28] have reported that since the traveling velocity (terminal velocity) of the particles based on interfacial tension migration is proportional to the diameter of particles, and is proportional inversely to the viscosity, when the interfacial tension gradient is constant, and particles are more far away from refractories wall, if the inclusion grows and its diameter becomes large, it has been said that the traveling velocity becomes high and tends to adhere the nozzle surface easily. From the above argument, it is expected that adhesion of the inclusion decreases by Shape② in which turbulence energy suppressed significantly.

4.1.3. Water model experiment for the TD upper nozzle

Supposing the actual system, upper nozzle, SG, and SEN were set to the experimental tank, and the mould was set to the lower part. Same as the high-speed conditions in previous flow analysis, the amount of flow per unit time (the flow velocity) set to 4.485ℓ/s. The upper nozzle used was usual porous type, and it had the structure from which gas flows out of the whole bore surface in the nozzle, and the air of 15ℓ_N/min was blown in the water model experiment. (Where ℓ_N, normal liter, is amount of flow at standard state of 0℃ and 1atm.) With the actual system, since the gas is blown at high temperature at around 1550ºC, it counts upon cubical expansion and it is thought that it becomes one several times the amount of capacity of this. Therefore, in the system, it is thought in a water model experiment that the conditions of 15ℓ_N/min are comparable to the amount of gas blowing in about 3 - 5ℓ_N/min for the actual operation. Although the diameter of blow out gas changes by the gas pressure and kind of fluid blowing out etc., it was about 1mm on the conditions which blow out the air of 10ℓ_N/min to water. Although the gas blow technology which described previously in the introduction part, has not all-round effect for the prevention from adhesion, even if a certain effect is accepted in reduction of adhesion by covering the nozzle surface by gas, it was utilized together with the present improvement in the nozzle bore profile. In the simulation in flow analysis, however it was not taken into consideration.

When the flow situation of the air blown into the stream is observed from the nozzle upper part for the Shape① and ②, respectively, as shown in Figure 13. In the Shape①, the blown air flows violently through the bore in the nozzle, spiral flow was also seen. The probability which air attains to the nozzle center is also very high, and it is thought by Shape① that the intense high turbulence with high kinetic energy has occurred in the nozzle bore. A flow of gas was very quiet and the air which blew off from the surface in the nozzle flew toward straight under by Shape② along the surface in the nozzle toward the nozzle outlet (bottom) mostly to it.

From this, by Shape②, the turbulence with high kinetic energy is not generated but it is thought that the comparatively steady flow was obtained.

(a) (b)

Figure 13. Comparison of the test results of water model simulation for the nozzle of Shape① (left) and Shape② (right) as the photograph taken from nozzle top with blowing gas.

4.1.4. Field test in the actual CC system in the steel works

The examination for the system to compare Shape① and ② was done to the same timing using the CC facility of two strands as shown in Figure 14, and the upper nozzle of Shape① was set to one strand of the two and by another strand in the upper nozzle of Shape②. The test was performed at the same conditions in both strands, such as SG and SEN other than the upper nozzle. In addition, as described previously, for the upper nozzle of Shape① and ②, an inert gas blowing was carried out for both using all porous type nozzle, as the case of the water model experiment. The gas blowing was controlled by the back-pressure of about 100kPa. The capacity of the ladle was 180ton and 6-cast was performed in the throughput (flow velocity) of 4.485ℓ/s which is the high-speed conditions in the previous flow analysis and water model experiment, corresponding to about 2ton/min for each strand.

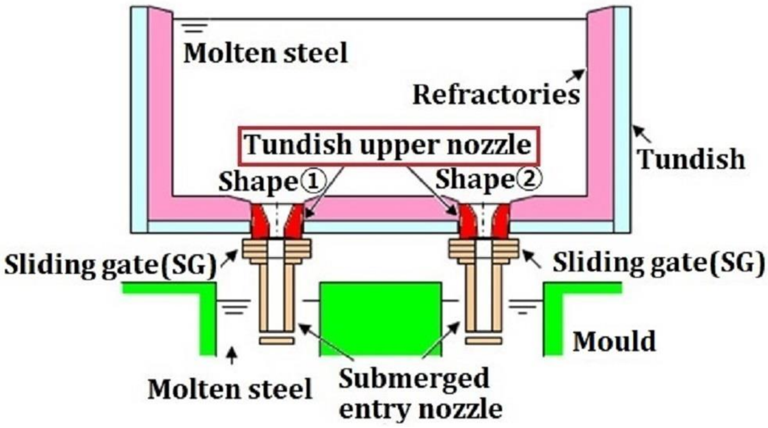

Figure 14. Set-up of test nozzles of Shape① and Shape② for two strands TD in the actual CC system in the steel works.

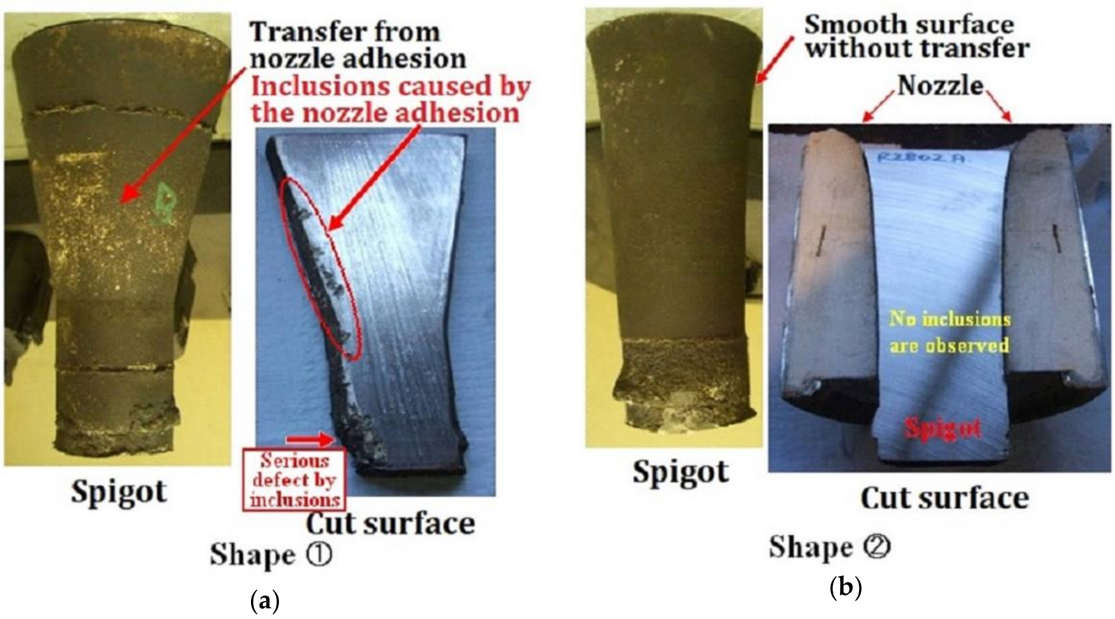

Figure 15. Comparison of the appearance of spigots obtained in the test.

Appl. Theory Comput. Technol. **2017**, 2, 4; doi: 10.22496/atct.v2i4.115

(a) (b)

Figure 16. Comparison of the cross section of the SENs connected from the upper nozzles of Shape① (a) and Shape② (b), respectively, 15 to 20mm thick adhesion is observed in (a) but no adhesion is observed in (b).

The solidified metal (spigot) which remained in the inner bore was investigated after casting. Although the metal which remained in the bore in the upper nozzle was shown in Figure 15. In the case of the Shape①, adhesion was seen at the corner part from which inner bore profile changes, and the nozzle lower part near the SG. On the other hand, in the Shape②, adhesion was not observed at all to it. Moreover, the quality of the cut surface of the spigot was also very smooth, and the contamination of the inclusion etc. was not seen. In the detailed observation after casting, and adhesion or erosion were not observed at all in the case of Shape②.

Although adhesion of 15-20mm thickness was observed in the inner bore of the SEN connected to Shape① as shown in Figure 16(a), adhesion was not observed at all in the inner bore of the submerged entry nozzle connected to Shape② as shown in Figure 16(b).

The improved prevention effect from adhesion due to suppression of condensation growth in the inclusions also might be brought by the increased flow velocity of the inner bore part, facilitating the air bubbles to downstream.

4.2. SEN

In the steel CC process, homogenization of molten steel flow in the mould is quite important for assuring quality of steel products. Since suppression of the adhesion of Al_2O_3 based inclusion to the ejection port and inner bore of the SEN as a final outlet of the molten steel to the mould is considered as key factor of stabilizing the molten steel flow in the port ejection, development of stepwise type [29] and mogul type [30] geometry of the SEN inner bore, application of SiO_2 [31] or B_2O_3 [32] as a substitution of Al_2O_3-C based SEN materials in conjunction with investigation on the improvement effect of the anti-adhesive in the case of CaF_2 [33] or CaO [34] addition to the ZrO_2 based materials, and multilayer type [35,36] nozzle structure have been tried in previous research works so far. Thus, from another points of view, application research of spinel-C based materials [37,38] to improve anti-erosion property of nozzle itself despite opposite of anti-adhesive property have been carried out, and effect of Ar gas blowing [39] on the adhesion, adhesion mechanism [40], device of evaluation method [41] of adhesion and case study of fluid analysis [42,43] of molten steel flow have been reported. However, despite of tremendous efforts described above, stabilization of port ejection flow in the SEN has not yet achieved.

4.2.1. Energy minimization theory and geometrical design of the SEN

Molten steel flow from the SEN inner bore to nozzle ejection ports is schematically shown by the arrows in Figure 17. In the figure, the controlled molten steel flow by the SG at the upper part of the

 Appl. Theory Comput. Technol. **2017**, 2, 4; doi: 10.22496/atct.v2i4.115

SEN vertically downward to the straight nozzle body (arrow (1) in the figure). Here in the coordinates vertical downward direction is +*Z* and direction of ejection port (horizontal direction) is ±*X*. Straight forward flow down velocity V in straight body part of the SEN vertically can be considered as $V \fallingdotseq V_Z$ (*Z* direction component of *V*) and $V_X \fallingdotseq 0$ (*X* direction component of *V*), although there is some possibility to induce a drift due to affection of flow controlling system in the upper stream side of the SEN. However, to decrease the flow velocity and stabilize the molten steel flow in the mould in which the SEN is installed, the ejection ports must be directed to almost horizontal becomes $V \fallingdotseq V_X$ and $V_Z \fallingdotseq 0$, that is a conversion of flow direction as shown in the arrow (2) in the figure. Therefore, it is important that the conversion of the flow velocity direction from $V=V_Z$ to $V=V_X$ is performed stably without losing energy during molten steel flow from inlet of ejection port (SEN inner wall side) to outlet of the ejection port through the part of ejection port.

Applying the Bernoulli's theorem as the energy conservation law for flow to the molten steel in the continuous casting mould, the following Eq. (9) can be obtained as same as the Eq. (2),

$$\rho V^2/2 + \rho g H + P = Const., \tag{9}$$

Where, density of molten steel, velocity of flow, gravitational acceleration, head (position in depth) and pressure are expressed by ρ, V, g, H and P, respectively. The first, the second and third terms of the left-hand side of the Eq. (9) indicate kinetic energy, position energy and hydrostatic pressure, respectively. Although no terms expressed in the Eq. (9) for energy loss in the flow, a considerably high energy loss occurs due to transformation of flow to turbulent by changing the flow direction abruptly as seen in the ejection port in the SEN.

In the ejection port of the SEN, since $H= X'$ (position toward inlet from the exit of ejection port) and $V=V_X$ (*X* component of flow velocity inside of ejection port), Eq. (9) can be also expressed as follows;

$$\rho V_X{}^2/2+(\rho g' X' + P + \alpha) = Const., \tag{10}$$

where, g' is gravitational acceleration in the ejection port and $g' = g \times \tan(\theta)$ when inclination angle of direction of ejection port flow root against horizontal line is θ. α is kinetic energy occurred in the ejection port except for X component ($V_Z{}^2$ and $V_Y{}^2$) including the energy loss occurred by formation of turbulent flow.

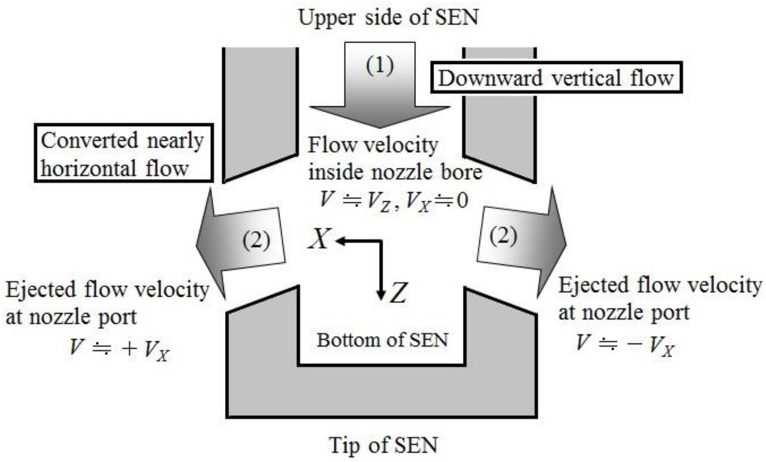

Figure 17. Schematic flow directions of molten steel in the SEN in which downward vertical flow described by (1) is converted to two of nearly horizontal flows described by (2).

The authors have already reported [1, 44,48] that a significant contribution can be given for the stability of the operation of continuous casting and of the steel quality with including some of test results in actual operation line through suppressing to minimum both occurrences of turbulent energy and adhesion of Al_2O_3 based inclusions to the nozzle by applying the energy minimizing theory which means energy loss minimization during molten steel flowing in nozzle, to the geometrical design for the TD upper nozzle.

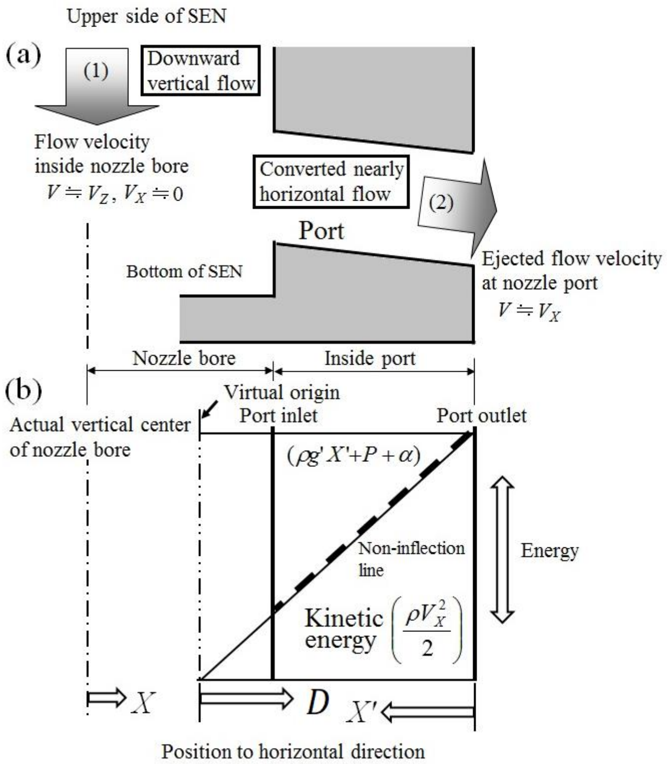

Figure 18. Explanatory illustration for ideal energy distribution (b) of the molten steel flow in the port of the SEN (illustrated schematically in (a)) based on theory of the energy minimization.

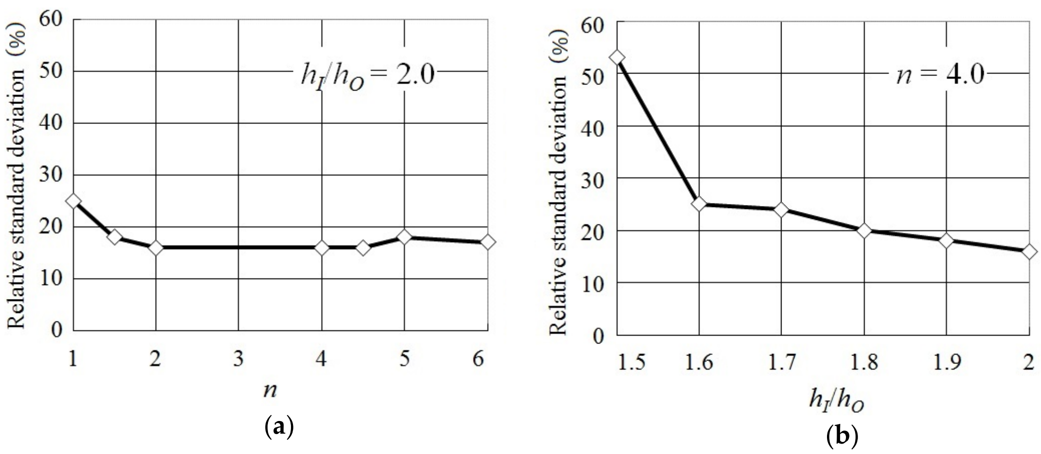

Figure 19. Analytical optimization of the parameters, n, h_I and h_O for determining the geometrical design of the SEN using relative standard deviation (= standard deviation/average) of the flow velocity in the port.

The energy minimization theory means in another word that the energy change for a period of molten steel passing the nozzle is able to express by a linear function without having an inflection point. Namely, as energy distribution during passing molten steel through the SEN is schematically shown in Figure 18, the second term in the left hand side of Eq. (10), ($\rho g' X' + P + \alpha$) equals to $V_X{}^2$ (kinetic energy) varied linearly with X', obtaining kinetic energy distribution of the linear function shown in the figure as "Non-Inflection Line", must be hold and the following relation must be hold.

$$V_D{}^2 \propto D, \tag{11}$$

Where D is distance from virtual origin imaged inside of inner bore of the SEN to direction toward exit of ejection port and V_D is the X component in the flow velocity (V_X) at the position D. On the other hand, for the molten steel passing through the ejection port following Eq. (12) on the continuity of the fluid.

$$Q = V_D \times A_D = Const., \tag{12}$$

Where, Q is rate of volumetric flow of molten steel, and A_D is the cross section of the ejection port at the position of D. Combining the Eq. (11) with the Eq. (12), the following relation is finally obtained as Eq. (13).

$$A_D \propto D^{-1/2}, \tag{13}$$

Equation (13) is a fundamental formula to be used for designing the geometry of ejection port to suppress occurrence of energy loss and turbulent flow to the minimum limit in molten steel flow in ejection port of the SEN and using the SEN designed based upon the prospect mentioned above, the turbulent flow is inhibited to the minimum limit in the part of ejection port and the low velocity and homogeneous velocity distribution can be obtained even at the outlet of the ejection port.

Thus, to generalize the Eq. (13) further, suppose the height of the ejection port in the D position is T_D when width of the ejection port is a constant, the relationship of $T_D \propto A_D$ is hold. Then the left-hand side of Eq. (13) is substituted to T_D, and if the exponential term of the right-hand side converted to more general form $-1/n$, the Eq. (13) can be rewritten as follows;

$$T_D \propto D^{-1/n}, \tag{14}$$

As the parameters to reflect the relation expressed by Eq. (14) to the actual geometry of the SEN, n for a degree of upper and lower curves in the cross-section diagram of the ejection port, h_I and h_0 for both height of inlet and outlet of the ejection port were selected. Where the h_0 is considered as a constant (setting value) with the relation of $h_0 \leqq T_D \leqq h_I$. In order to optimize conditions of these values for stabilizing the ejection flow velocity V_x at the outlet of the ejection port, the effect of these parameters on the fluctuation factor (ratio of standard deviation and average value) of the V_x was investigated analytically. At first analytical results for varying n value for the condition of h_I/h_0=2.0 is shown in Figure 19(a). In the figure, since the fluctuation factor is low and stable in the condition of $2 \leqq n \leqq 4.5$, the effect of the fluctuation factor with varying h_I/h_0 was checked with selecting $n = 4.0$. As the result, it was clarified that the fluctuation factor is low and V_x tends to stabilize in the condition of h_I/h_0 higher than 1.6 as shown in Figure 19(b).

Where, the other conditions for the numerical analysis mentioned above were that inner and outer diameters of the SEN were 70 and 130mm, respectively, the ejection port is round shape with inclination angle of 20deg. from horizontal, and finally mould size and flow rate of the molten steel are 220×1800mm and 5ℓ/s, respectively.

4.2.2. Flow analysis for the SEN by CFD

A fluid analysis on the SEN has been performed by Thomas and Bai [43] comprehensively on the upper stream controlling system and effect of blowing gas and adhesion on the molten steel flow. However, they have never reffered to the geometry of the ejection port. Although authors have already reported the results of flow analysis [2] on unique structure having protrusion like guides in both sides from the height position of the ejection port of the SEN to the outlet of the ejection port

 Appl. Theory Comput. Technol. 2017, 2, 4; doi: 10.22496/atct.v2i4.115

through the inner bore part, it was clarified that occurrence of turbulent flow is higher in the ejection port having the unique structure compared to the conventional structure and also reducing effect of the MPV is low. In the present invesitigation a new geometry of the ejection port which was designed by applying above described energy minimization theory on the SEN with typical conventional structure of the ejection port have been analysed.

Conditions for numerical calculation such as the geometry and size of ejection port, depth of immersion, mould size of CC and rate of molten steel (throughput) are shown in Table 2. Geometry of part of ejection port showing vertical cross section including a line connecting the center part of both ejection ports in the cross section of SEN of only bottom right side are shown in Figure 20(a) and (b) for "Shape③" and "Shape④", respectively. Where a turbulent flow calculation using the fluid anaysis software FLUENT12.1.4 was performed for both shapes of the SEN, they are conventional geometry of Shape③ and Shape④ which is derived from the above described energy minimization theory. The Shape③ is a geometry aiming to suppress the occurrene of negative pressure and back flow at the upper part of the ejection port by adapting the DTP corner cut in the upper inside of the ejection port. In the Shape③ the effect of lowering of the MPV has been expected by a deep well structure in which the setting height of ejection port is the position of 50mm from the bottom of the SEN inner bore as shown in Figure 20(a). Here an inclination angle of the ejection port from the horizontal line was set to downward 25 deg. commonly for both shapes. In the case of Shape ④, width of ejection port was set constant as 88mm and the height of ejection port inlet was set

Table 2. Conditions of the numerical analysis.

Cross section of mould for continuous casting	Width×thickness= 1372×230mm
Throughput of molten steel	6 ℓ/s
Submerged depth (from meniscus to the tip of SEN)	290mm
Dimensions of the submerged entry nozzle and the installed ports	Length×outer dia.×inner dia=847×150×90mm Cross section of ports; width×height=88×70.6mm
Downward inclination angle of the ports from the horizontal line	25 deg.

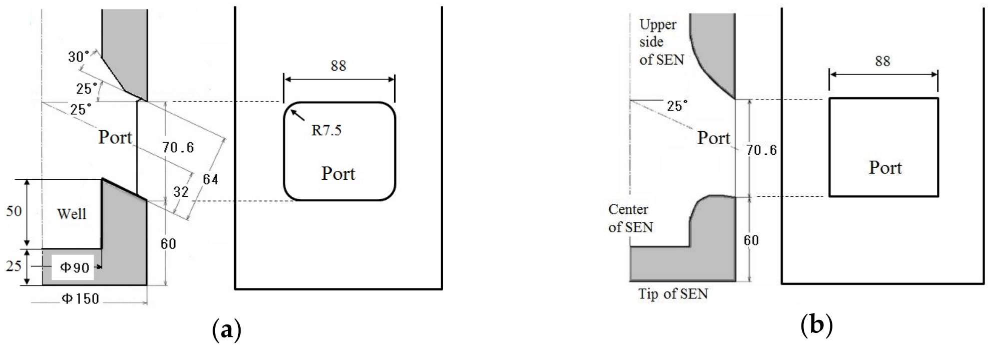

Figure 20. Shape and dimension of port in the SEN as representative right-half profile (section) (in the left hand) and front view of the port (in the right hand) for numerical analysis of molten steel flow in the continuous casting; in (a) conventional (DTP) type nozzle as Shape③ and (b) newly designed one as Shape④.

as 141.2mm which is derived from h_1/h_0=2.0 according to Figure 19. And also adapting optimum solution 4 for n in the relation expressed by Eq. (14) , the height of ejection port at the position D of the SEN radial direction, T_D follows the relation; $T_D \propto D^{-1/4}$. The water liquid was used for calculation since its Reynolds number is almost equal [45-47] to that of molten steel. Center axis of the SEN is set as X=Y=0mm with width direction (direction of ejection in the ejection port) as ±X and mould

 Appl. Theory Comput. Technol. 2017, 2, 4; doi: 10.22496/atct.v2i4.115

thickness direction as *Y*, and molten steel surface in the mould as *Z*=0mm in the vertical direction which is set +*Z* as the downward direction.

Figure 21 shows two-dimensional flow velocity distribution in the center cross section of the mould (*Y*=0mm) and in Shape③ (a) the flow velocity in the lower part of ejection port is high (yellow ~red colour) with colliding almost linearly to both left and right side walls in the mould. Molten steel flow from meniscus to ejection port is also seen in (a) which is considered to caused by negative pressure occuring in the upper part of ejection port. On the other hand, in Shape④ (b) the flow is homogeneous and low velocity (green colour) in whole ejection port and the colliding flow velocity to the both left and right-side walls in the mould is decreased by decreasing MPV and velocity of the ejection after flow.

Three-dimensional distribution of the flow velocity vectors in the outlet of ejection port is shown in Figure 22(a) and (b). As is apparent from the figure, in Shape③ (a), considerably large velocity difference in upper and lower positions of the ejection port is observed even though the DTP & deep well type which is thought as a superior geometry among the various types of conventional geometry used so far. However, the flow velocity distribution obtained here should be considered as even excellent. In the meantime, the flow velocity seems to be remarkably homogenized in whole ejection port of Shape④ (b).

Variations of the ejection flow velocity (V_X: *X* component flow velocity) with position in depth of the ejection port for both Shape③ and Shape④ were shown in Figure 23(a) and (b), respectively, to investigate some detail in the ejection flow for both types of port geometry. Results of the analysis for both types are shown in the inserted table in the figure where the Shape④ exhibited a highly homegenized state of flow in the whole part of the ejection port with largely improved ejection flow property in which the minimum value of the flow velocity "Min." is high and the standard deviation of it, "Deviation" is reduced to about half even though the lowering of the maximum value "Max." is meager compared to the case of Shape③. There are some difference in the average value of the flow velocity, "Average" for both Shape③ and Shape④. As the cause of such difference, homogeneity in the rate of ejection flow for both left and right ports was much higher in the Shape④ in which the rate was 2.997 and 3.003ℓ/s for +*X* and -*X* sides, respectively, compared to the case of Shape③ in which the rate was 3.025 and 2.975ℓ/s for +*X* and -*X* sides, respectively, about 1% high rate in the +*X* side. Also as an another reason it is considered that there was slight difference in the geometry of the ejection port in the calculation model, as was shown in the Figure 20(a) and (b), the corner radius (R7.5mm) is set in the outlet of the ejection port in the Shape③ (a), but not in the Shape④ (b), resulting in the slight increase in the cross section in the Shape④.

Two-dimensional distribution of turbulent kinetic energy in the mould and nozzle center cross section (*Y*=0mm) for Shape③ and Shape④ are shown in Figure 24(a) and (b), respectively. As seen in the figure, it is clarified that the turbulent kinetic energy for Shape③ in (a) is quite high in the position of the bottom part of the SEN, especially in the lower inlet of the ejection port. The occurrence of the turbulent flow facilitates the adhesion of the inclusion in the molten steel to the surface of nozzle materials and increases the wear loss by the erosion of the nozzle due to increased contact probability of the inclusion. Namely, the adhesion and/or erosion wear into the SEN materials makes the molten steel flow from the ejection port to the mould further instable state due to serious change of the ejection port from its original geometry. And also, once adhesion occurred in the nozzle, an abrupt change is brought on the molten steel flow from ejection port to the mould by spalling due to

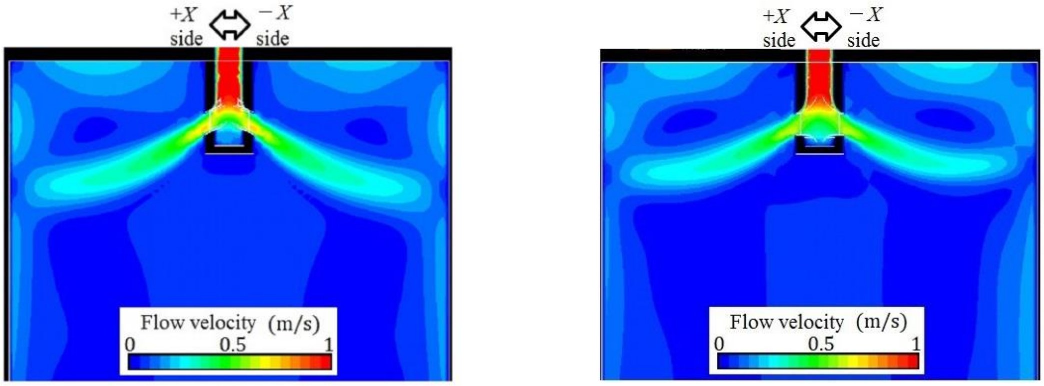

(a) (b)

Figure 21. Flow velocity distribution (at Y=0mm) of the molten steel poured into the mould through the SEN located upper center part of the images for (a) Shape③ and (b) Shape④, respectively.

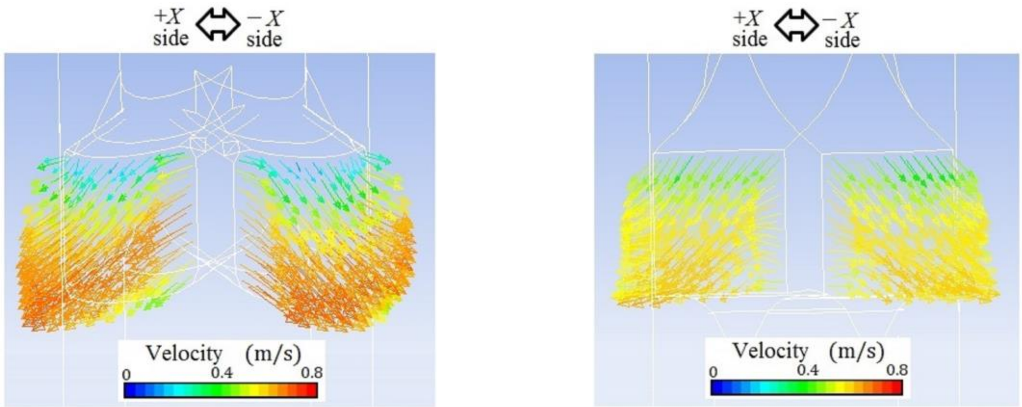

(a) (b)

Figure 22. Three-dimensional velocity vectors distribution calculated by CFD at the outlet of the ports of the SEN for (a) Shape③ and (b) Shape④, respectively.

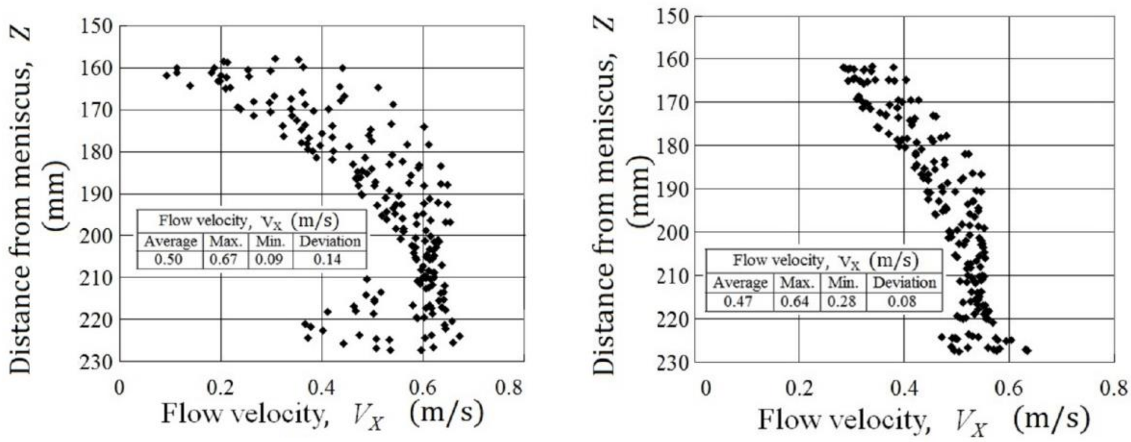

(a) (b)

Figure 23. Variation of the flow velocity (Vx) at the +X side port outlet with Z (distance from meniscus) for (a) Shape③ and (b) Shape④, respectively, and results of calculation are shown in the inserted table as average, maximum, minimum and deviation of the flow velocity comparing (a) with (b).

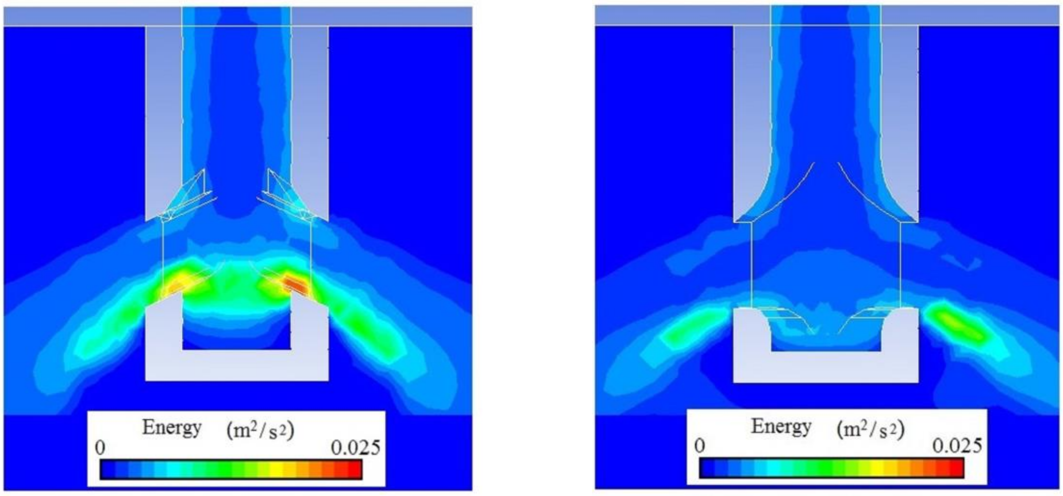

(a) (b)

Figure 24. Two-dimensional distribution of the turbulent kinetic energy at Y=0mm section in the nozzle and mould calculated by CFD for (a) Shape③ and (b) Shape④, respectively.

impact of the flow. For the worst case of the adhesion, the operation is forced to stop by clogging of the nozzle. On the contrary the highly expectable results of analysis were obtained for the Shape④ in Figure 24(b) where the suppression effects of the generation and growth of the inclusions, their adhesion to the nozzle surface and the erosion wear, have been realized by stabilizing and homogenizing the ejection flow using newly designed SEN.

4.2.3. Water model experiment for the SEN

The water model experiments were carried out by the same condition as the flow analysis in the previous section. Where in order to play a role of a tracer in taking photographs and the particle image velocimetry (PIV), air was blown by the rate of $2\ell_N$/min. from the porous upper nozzle installed in the upper part of the SG. The diameter of the air bubbles generated in the mould was about 1-3mm. The relatively large bubbles tend to surfacing upward by the action of the buoyancy with separating from the direction of the water flow in the mould. On the contrary, the direction of water flow is also considered to be shifted upward by the effect of the bubble movement. According to the results on the optimization of the amount of blowing gas in the case of the TD upper nozzle [50], the rate of blowing of the air was lowered to the possible limit in order to minimize the effect of the bubbling on the water flow. The flow behaviour in the mould for Shape③ and Shape④ were compared by the photographs shown in Figure 25(a) and (b). Although they are somewhat hard to see with the low contrast monocolour photographs, it was able to confirm that the flow was kept low velocity in the whole mould for the Shape④ in the water model experiment shown in the Figure 25(b) as same as the results of the CFD analysis shown in the Figure 21(b). To compensate the unclearness in the Figure 25, the measured data images of the flow velocity using PIV in the cross section of center of mould thickness direction (*Y*=0mm) were compared in Figure 26(a) and (b) for Shape③ and Shape ④, respectively. The figure shows the average value of the PIV measurement during stroke of 1min., and the maximum ejection flow velocity (MPV) for both cases were 0.60 and 0.52m/s for Shape③ and Shape④, respectively, showing the almost similar results as the CFD analysis again. However, in the PIV measurements there was a tendency to lower the flow velocity compared to the value of the actual MPV because of averaging the whole data obtained. The direction of the ejected after flow is somewhat upward in Shape④ as was confirmed in both images of the Figures 25 and 26, exhibiting a same tendency as in the CFD analysis described in the previous section.

Assuming the operation with the higher speed casting, water model experiments were also performed at the flow rate of 12ℓ/s which is twice as high as the previous experiments. MPV results obtained by the PIV measurements were 1.08 and 0.74m/s for the Shape③ and Shape④, respectively. Superiority on the homogenizing the ejection flow in the Shape④ became much higher in the condition of the higher rate of flow compared to the case of lower one, resulting in the increase expectation on the further improvements in the productivity and product quality.

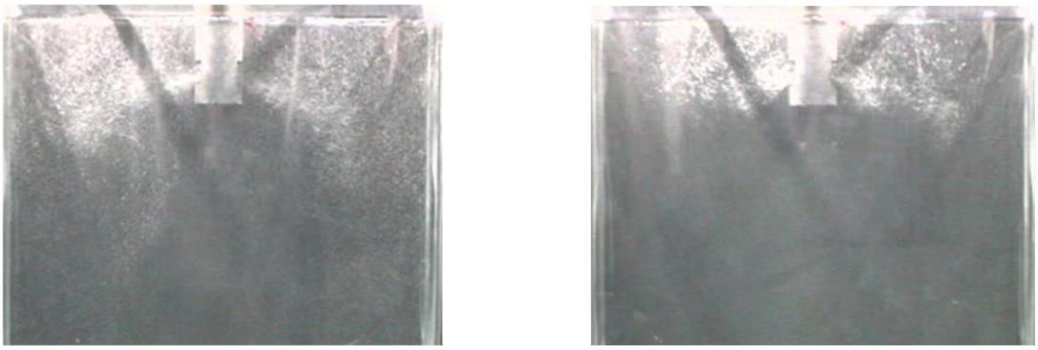

(**a**) (**b**)

Figure 25. Bubbled gas-visualized water flow from the SEN located upper center part in the photo of water model experiments for the cases of (a) Shape③ and (b) Shape④, respectively.

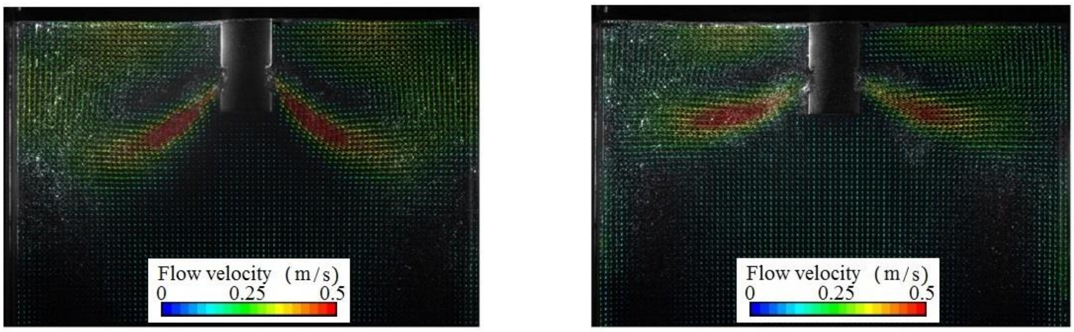

(**a**) (**b**)

Figure 26. Particle image velocimetry (PIV) expressing water flow from the SEN located upper center part in the water model experiments as calculated average measured data at Y=0mm section during 1 min measuring term for (a) Shape③ and (b) Shape④, respectively.

4.2.4. Discussion

In the analytical results for the geometrical design previously shown as the Figure 19(b), the fluctuation factor for flow velocity was kept in the lower value when h_1/h_0 is higher than 1.6 and indicating the tendency to stabilizing the velocity much better for further high value. However, there is a limit for the value of h_1 due to constraint in the length and manufacturing of the SEN. Therefore in the geometrical design for the Shape④ the h_1 set the highest value as possible as following h_1/h_0=2.0. And n was set to 4.0 in order to keep the straightness of the molten steel flow at the ejection port. Although the analytical calculation was also performed in the same condition for the value of h_1/h_0=1.0 which is representing the conventional geometry, the fluctuation factor of the flow velocity was as high as 85%.

 Appl. Theory Comput. Technol. **2017**, 2, 4; doi: 10.22496/atct.v2i4.115

As the results of the flow analysis performed in the same condition to obtain the calculation results shown in the Figure 19, the difference of the state of flow in the part of the ejection port of the SEN for both conventional geometry and new geometry determined by energy loss minimization theory is shown in Figure 27 for three-dimensional distribution of the flow velocity vectors in the part of ejection port, and in Figure 28 for two-dimensional distribution of turbulent flow energy in the cross section of the ejection port. As apparently shown in the figures, the ejection of the flow is rather concentrated in the lower part of the port and the backward flow occurred in the upper part (see Figure 27(a)) with exhibiting an intensive occurrence of the turbulent flow as seen in the Figure 28(a). In contrast to the above results, as seen in the Figures 27(b) and 28(b), the ejection of the flow is homogeneous with low velocity and free from the occurrence of turbulent flow in the case of the nozzle designed by the theory on the energy loss minimization. Thus, it is important that the height of the ejection port T_D at the position D of radial direction of the nozzle is assured by changing height position of the upper and lower surfaces of the ejection port to keep the center line of the direction of the height in ejection port setting to the inclination angle.

Since the new geometry Shape④ is much effective for the homogenization of the ejection flow velocity at the higher speed condition (12ℓ/s) from the results of water model experiments, the state of the flow at the high speed condition was also analyzed by the CFD, and the results are shown in Table 3. In the comparison to the results obtained in the casting speed of 6ℓ/s as was shown in the Figure 23, the lowering of the MPV, "Max." was also comfirmed to be significant in the high speed condition for the Shape④ by the numerical calculation. For the minimum value "Min." of the flow velocity was 0.10 and 0.55m/s for Shape③ and Shape④, respectively, with having 5 times difference.

The regression analysis results of V_X distribution in the vertical (height) position of Z=195mm (Y=0mm) (see Figure 29; center of the outlet of the ejection port), distance from center of the SEN to the outlet of the ejection ports of left and right sides (±X sides) are shown in Figure 30(a) and (b) for Shape③ and Shape④, respectively. It wa slso confirmed in the Figure 30(b) that an ideal velocity distribution with free from the inflection point from the center of the SEN to the ejection ports in the left and right sides (±X sides). According to the analytical results obtained in the Figure 30, it was able to consider that the occurrence of the turbulent flow was suppressed to the minimum limit for the new geometry (Shape④), resulting in the homogeneous distribution of molten steel ejection in whole part of the ejection port.

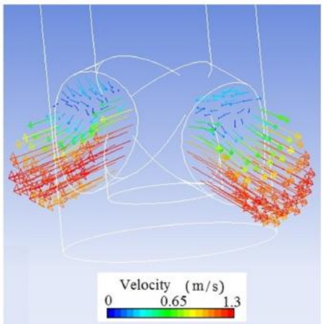

(a)

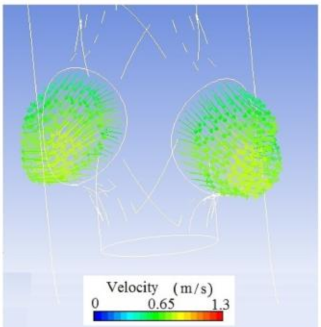

(b)

Figure 27. Three-dimensional distribution of the velocity vectors calculated by CFD in the condition described previously for Figure 19, showing for (a) conventional shape nozzle (h_I/h_O=1.0) and (b) newly design nozzle (h_I/h_O=2.0, n=4), respectively.

Appl. Theory Comput. Technol. 2017, 2, 4; doi: 10.22496/atct.v2i4.115

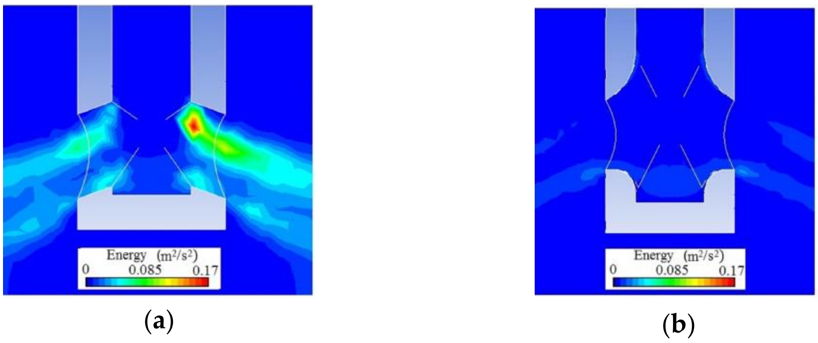

Figure 28. Two-dimensional distribution of the turbulent kinetic energy for (a) conventional nozzle (h_I/h_O=1.0) and (b) newly design nozzle (h_I/h_O=2.0, n=4), respectively.

Table 3. Calculated flow velocity obtained by CFD analysis for higher throughput (12ℓ/s).

Nozzle design	Flow velocity, V_X (m/s)			
	Average	Maximum	Minimum	Deviation
(a) Shape③	0.98	1.41	0.10	0.30
(b) Shape④	0.94	1.25	0.55	0.18

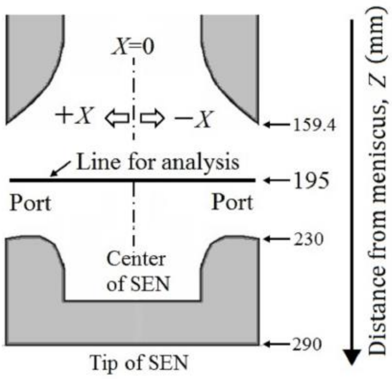

Figure 29. Position (Z=195mm) of flow velocity V_X distribution analysis.

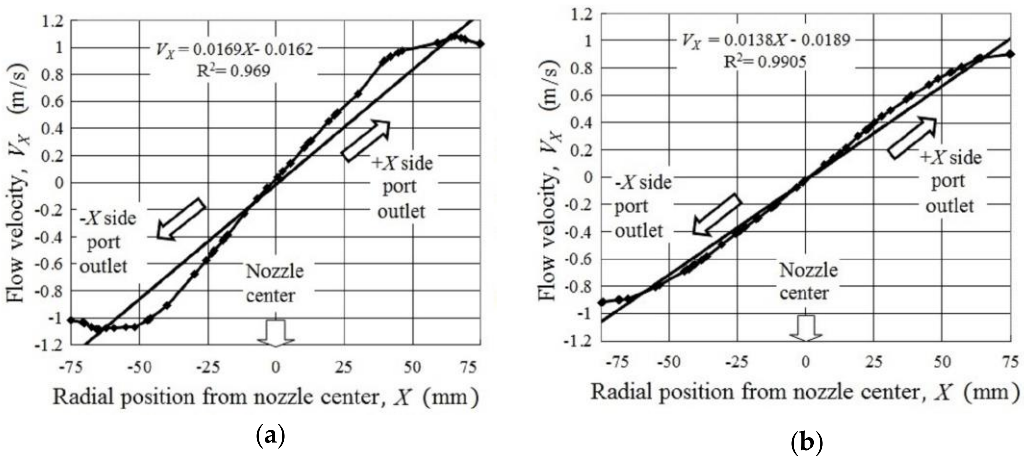

Figure 30. Comparison of X-component flow velocity V_X distribution from center (X=0mm) of the SEN to outlet of both ports (+X and -X directions) at Z=195mm (Y=0mm) calculated by CFD in the condition of higher throughput (12ℓ/s) for (a) Shape③ and (b) Shape④, respectively.

5. Concluding Remarks

The bore shape of the TD upper nozzles in CC facility of the steel, was investigated based on the basic principle of hydrodynamics, aiming to suppress the turbulence with high kinetic energy generated in the molten steel flow. The optimal nozzle bore profile (4th curve) was determined as the function of the molten steel head (height) and nozzle radius which derived from the principle of the energy minimum in the molten steel flow. The simulation by flow analysis and water model experiment was first performed for both shapes of this 4th curvilinear nozzle and conventional one. It was clarified that generating of the turbulence with high kinetic energy can be controlled in the upper nozzle which made the inner bore profile the 4th curve (curved surface) of alignment. Furthermore, when the actual nozzle was made as an experiment for the trial in the actual steel works was presented with the conventional shape nozzle for comparison, with the 4th curvilinear shape upper nozzle, it became clear that it not only can control the adhesion of the inclusion to itself, but it demonstrated the adhesion control effect also in the SEN installed in the lower stream side. By application of the nozzle newly devised from this, not only the durability improvement of the refractories in the molten steel CC process but both the slanted flow within the mould generated by alumina adhesion and the contamination due to mixing the exfoliated inclusions decreased, and it was thought that it could contribute to the improved quality of steel or operation stabilization.

Optimization of geometry of ejection port of the SEN has been performed in order to stabilize the velocity of the molten steel flow in the mould for CC of steel through suppressing the energy loss in the molten steel flow passing the ejection port of the nozzle to the minimum limit with device of newly designed geometry of the port utilizing theory of fluid mechanics. In the newly designed SEN, analysis by CFD as well as water model experiment apparently verified the effectiveness for suppressing turbulent flow and homogenizing the flow velocity. Application of the new geometry SEN to the CC operation reduced the MPV and the occurrence of the negative pressure at the upper part of the ejection port with inhibiting back flow, resulting in stable molten steel flow in the mould. Stabilizing molten steel flow by suppressing the turbulent flow bring to improvement of both adhesive of inclusion to the nozzle surface and erosion/corrosion of the nozzle surface.

Acknowledgements: The authors appreciate BlueScope Steel Ltd. located in Wollongong, Australia which cooperated with the valuable field tests on the TD nozzle in their steel works. We also appreciate TARJ (Technical Association of Refractories, Japan) and RAN (Refractories Applications and News) kindly approved re-submission of a part of the paper on the TD upper nozzle which was published in their journal.

Author Contributions: Dr. Arito Mizobe conceived the research theme based upon abundant experiences on the flow analysis of the molten steel. He also conducted the water model experiments with Mr. Jouji Kurisu. They also discussed on both experimental and analytical data. Dr. Masanori Ueki contributed in literature review, total discussion and paper writing.

Conflicts of Interest: The authors declare no conflict of interest.

Nomenclature

A Bore cross-cectional area in TD upper nozzle m^2
A_D Cross section of SEN ejection port at position D m^2
D Distance from the virtual origin to the position in the exit direction of SEN ejection port m
d Diameter of TD upper nozzle (= $2R$) m
g Gravitational acceleration m/s^2

g' Gravitational acceleration in the direction of SEN ejection port ($g\times\tan(\theta)$) m/s^2
H Head (Location in tundish (TD) or mould depth) m
H_r Height (depth) from the meniscus in the TD m
h_I Height of inlet of ejection port (inner bore side of SEN) m
h_0 Height of exit of ejection port (outer surface of SEN) m
n Degree of upper and lower curves in the cross section of SEN ejection port
P Hydrostatic presure Pa
P_0 Hydrostatic pressure at meniscus (surface) in the TD Pa
P_1 Hydrostatic pressure at nozzle outlet in the TD Pa
Q Rate of volumetric flow of molten steel m^3/s = ×10^3 ℓ/s
R Radius of TD upper nozzle m
R_e Reynolds number
T_D Height of SEN ejection port at position D m
V Velocty of molten steel flow m/s
V_0 Velocity of molten steel flow at meniscus (surface) in the TD m/s
V_D Velocity (V_X) of molten steel flow in the SEN at position D m/s
V_X X component of velocity of molten steel flow m/s
V_Y Y component of velocity of molten steel flow m/s
V_Z Z component of velocity of molten steel flow m/s
U Average velocity of molten steel flow m/s
w Width of SEN ejection port m
X Direction of SEN ejection port (horizontal) (Center of SEN X=0) m
X' Position toward inlet from exit of SEN ejection port m
Y Direction of mould thickness (horizontal) (Center of SEN Y=0) m
Z Vertical direction (height of meniscus in the mould Z=0, lower direction: +Z) m
α Kinetic energy in the Y and Z directions, plus energy loss (for SEN) Pa = (m^2/s^2) ×(kg/m^3)
θ Inclination angle of the SEN ejection port from horizontal direction deg.
ν Coefficient of kinematic viscosity of fluid m^2/s
ρ Density of molten steel kg/m^3
X_{TD} Sliding direction of the SG (slide gate) mm
Y_{TD} Direction perpendicular to the sliding direction of the SG mm
Z_{TD} Height Direction in the tundish (TD) mm

References

1. Mizobe, A., Yasuda, T., Ueki, M. and Arimitsu, E., Optimum geometry of the tundish upper nozzle for the continuous casting of steel, *Proc.MS&T '10*, 2010, Huston, USA,pp.1727-1738.
2. Kuroda, T., Mizobe, A. and Kurisu, J., Flow optimization in the mould by port design improvement of submerged entry nozzle, *Proc. UNITECR'11*, 2011, Paper No.1-B2-16.
3. Hernandez, C. A., Barron, M.A and Miranda, R., Anchor-Shaped Design of a Submerged Entry Nozzle for the Continuous Casting of Steel, *Open Journal of Applied Sciences*, 2016, 6, 593-600 http://www.scirp.org/journal/ojap ps
4. Hernandez, C. A., Miranda, R. and Barron, M.A, Numerical Comparison of the Performance of Submerged Entry Nozzles for Slab Continuous Casting, *Int'l Conf. Modeling, Sim. and Vis. Methods | MSV'16 |pp74-77.*
5. Mohammadi-Ghaleni, M., Zaeem, M.A., Smith, J.D. and O'Malley R., Computational Fluid Dynamics Study of Molten Steel Flow Patterns and Particle-Wall Interactions Inside a Slide-Gate Nozzle by a Hybrid Turbulent Model, *Metallurgical and Materials Transactions B*, 47, Oct. 3056-3065 (2016).

6. Zhang, L. and Thomas, B. G., Application of Computational Fluid Dynamics to Steel Refining and Casting Processes, *Fourth International Conference on CFD in the Oil and Gas, Metallurgical & Process Industries SINTEF / NTNU Trondheim*, Norway 6-8 June 2005
7. Al-Dhafeery, Y.R., Modeling of Argon-Molten Steel Flow in a Slab Continuous Caster by Discrete Phase Model, *A thesis submitted to the degree of Masters of Engineering,* McGill University, Montreal, April 2012
8. Mishra, P., Ajmani, S.K., Kumar, A. and Shrivastava, K.K., Review Article on Physical and Numerical Modelling of SEN and Mould for Continuous Slab Casting, *International Journal of Engineering Science and Technology (IJEST)*, Vol. 4 No.05 May 2234-2243(2012)
9. Motaman, S., Mullis, A.M., Cochrane, R. F. and Borman, D. J., Use of Computational Modelling For Investigation the Effect of Melt Delivery Nozzle Tip Length on Gas Flow Separation in Supersonic Gas Atomization, *ICLASS 2012, 12th Triennial International Conference on Liquid Atomization and Spray Systems*, Heidelberg, Germany, September 2-6, 2012
10. Chatterjee, D., CFD Model Study of a New Four-Port Submerged Entry Nozzle for Decreasing the Turbulence in Slab Casting Mold, *ISRN Metallurgy*, Hindawi Publishing Corporation, Volume 2013, Article ID 981597, 6 pages, http://dx.doi.org/10.1155/2013/981597
11. Allen, P., Shields, C and Wilczynski, F., Optimisation of Nozzle Geometry in Bubbly Flow in the Continuous Casting of Steel, CDT Fluid Dynamics, University of Leeds, Supervisors: Bokhove, O, Jones, C. Fairweather,M., and Smith, C (Materials Processing Institute)
12. Goldschmit, M.B., Ferro, S.P. and Mazzaferro, G., Numerical modeling of liquid steel flow with free surface, *4th. European Casting Conference*, Birmingham, UK,. (2002).
13. Goldschmit, M. B., Ferro, S.P. and Owen, H.C., On the modeling of liquid steel processes, *Latin American Applied Research*, 32, 267-273(2002)
14. Chen, D.F., Jin, X., Zhang, D.J., Zhang, L.F., Xie, X., Zhang, X.G., Zhang, F.E. and Long, M.J., Water Model Simulation for Flow State in Slab Continuous Casting Mold, *Materials Science and Technology (MS&T*2009*)*, Oct. 25-29, 2009, Pittsburgh, Pennsylvania, USA.
15. Halliday, I. M. D., Continuous Casting at Barrow, *J. Iron and Steel Inst*., 1959,Volume 191,No.2, pp.121-163.
16. Morita, Z. and Adachi, A., A Consideration on Density and Viscosity of Fe-C System Molten Alloys and Their Structural Modification(Structure and Physical Properties of Liquid Metals), *Bussei-Kenkyu*, 1970,Volume 15,No.2, pp. 64-72(in Japanese).(Compiled in KURENAI: Kyoto University Research Information Repository, http://repository.kulib.kyoto-u.ac.jp/dspace/bitstream/2433/88184/1/KJ00004749025.pdf.)
17. Watanabe, K., *Fluid Dynamics-Flow and Loss-, Fundamental Mechanical Engineering Course,* Maruzen, Tokyo, Japan, 2002, p.51 (in Japanese).
18. Nippon Steel Monthly, July 2004, pp5-8(in Japanese).
19. Mizobe, A., Thermal and Mechanical Stress Analyses on the Manufacturing and Application Technology for the Refractory Materials, *Doctor Thesis for Hokkaido University*, Sapporo, June 2011, p.4 (in Japanese).
20. Thomas, B.G., Study of Transient Flow Structures in the Continuous Casting of Steel(1998-2001), *Final Report NSF Grant DMI-98-00274*, Jan. 31, 2002.
21. Tomita, Y., *Fluid Dynamics*, Yokendo, Tokyo, Japan,1971, p.112, p.115 (in Japanese).
22. Yamane, R., *Technology of Flow, Fundamental Mechanical Engineering Course,* Maruzen, Tokyo, Japan, 2003, p.76-78, (in Japanese).
23. Nakaoka, T., Agglomeration Simulation of Small Inclusion Particles in Molten Steel, *R&D Kobe Steel Engineering Reports*, 2006, Volume 56, No.1, pp.40-43(in Japanese).
24. Higashitani, K., Yamauchi, K., Matsuno, Y. and Hosokawa, G., Turbulent Coagulation of Particles Dispersed in a Viscous Fluid, *J. of Chem. Eng. of Japan*, 1983, Volume16, No.4, pp.299-304.

25. Taniguchi, S. and Kikuchi, A., Mechanisms of Collision and Coagulation between Fine Particles in Fluid, *Tetsu-to-Hagane(J. Iron and Steel Inst. Japan)*, 1992, Volume 78, No.4, pp.527-535 (in Japanese).
26. Shimasaki, S., Wada, T. and Taniguchi, S., Characteristics of Flotation, Sedimentation and Entrainment of Particle in Agitated Liquid, *Tetsu-to-Hagane*, 2003, Volume 89,No.6, pp.637-644(in Japanese).
27. Shimasaki, S., Wada, T. and Taniguchi, S., Slip Velocities of Solid Particles in Turbulently Agitated Liquid, *Tetsu-to-Hagane*, 2004, Volume 90, No.8, pp.538-545(in Japanese).
28. Mukai, K., Tsujino, R., Sawada, I., Zeze, M. and Mizoguchi, S., Effect of Refractory Materials on Inclusion Deposition of Immersion Nozzle in Continuous Casting and Mathematical Modeling of Inclusion Deposition, *Tetsu-to-Hagane*, 1999,Volume 85,No.4, pp.307-313(in Japanese).
29. Tsukamoto, N., Takai, M., Nomura, O., Ogata, M. and Lin, W., Prevention of alumina clogging in submerged entry nozzles, *Shinagawa Technical Report*, 2001,No.44,pp.27-38(in Japanese).
30. Colucci, P., Halloucherie, M., Leclercq, F., Verrelle, D.. Schiltz, C., Iida, E. and Nakamura, M., Improvement of meatllurgical qualities of florange steels by the use of mogul submerged entry nozzles, *Shinagawa Technical Report*, 2008,No.51, pp.9-18.
31. Takahashi, S. and Yamauchi, T., Application of anti-clogging material for SEN ports, *Taikabutsu(Journal of Technical Association of Refractories, Japan(TARJ)),* 2005,Volume 57,No.3, p.126(in Japanese).
32. Saito, M., Sorimachi, K., Sakuratani, T. and Kitano, Y., Effect of refractory materials on clogging phenomena of immersion nozzle, *CAMP-ISIJ*, 1991,Volume 4,No.1,p.222(in Japanese).
33. Ogata, K., Hiraiwa, Y., Uchinokura, K., Hanagiri, S., Ohtsuka, Y. and Fujiwara, S., CaF_2 addition to zirconia-mullite-alumina-graphite submerged nozzle: A solution to avoid clogging, *Taikabutsu*, 1993,Volume 45,No.11,p.638(in Japanese).
34. Nakamura, T., Takasu, T., Aoki, T. and Okumura, N., Effect of silica addition to anti-alumina clogging material, *Taikabutsu*, 1991,Volume 43, No.3,pp.120-123(in Japanese).
35. Osanai, H., Hasunuma, J., Nabeshima, S., Park, H. K., Benson, P. M., and Shinryo, M., Developement of new carbon free submerged nozzle for prevent alumina clogging, *CAMP-ISIJ*, 1997,Volume 10,No.1,p.177(in Japanese).
36. Yoshikawa, M., Ohtani, T., Ichikawa, K., Nakamura, R. and Uchida, S., Layer thickness to reduce the thermal stress generated in multilayered submerged entry nozzles, *Taikabutsu*, 1996, Volume 48,No.11,p.575(in Japanese).
37. Hata, M., Takahashi, S. and Uchida, K., The application results of spinel-graphte materials for the submerged entry nozzle, *Taikabutsu*, 2002,Volume 54, No.9,pp.469-473(in Japanese).
38. Nomura, O., Izaiku, T., Uchida, S. and Lin, W., Hot face observation of spinel-C SEN used for casting of high-oxygen steel, *Taikabutsu*, 2001,Volume 53,No.5,pp.304-305(in Japanese).
39. Mukai, K., Matsuoka, K., Wang, Z. and Lee, I., Influence of Ar gas injection on the involvement of mold powder, *CAMP-ISIJ*, 1997,Volume 10,No.4,p.805(in Japanese).
40. Choudhary, S. K. and Khan, A. J., Nozzle clogging during continuous slab casting at Tata Steel, *Steel Times Int.*, 2000,Volume 24, No.3,pp.21-22,pp.24-25,p.28.
41. Yamada, Y., Tsutsui, Y. and Kanematsu, K., Evaluation method on alumina buildup of submerged nozzle, *Taikabutsu*, 1993,Volume 45, No.3,pp.142-149(in Japanese).
42. Najjar, F. M., Finite-element modelling of turbulent fluid flow and heat transfer through bifurcated nozzles in continuous steel slab casters, *Proc. Electro. Furn. Conf.*, 1992,Volume 49,No. 1991,pp.401-405.
43. Thomas, B.G. and Bai, H., Tundish nozzle clogging-Application of computational models, *Proc. Iron and Steel Society*, 2001,No.18,pp.895-912.
44. Mizobe, A., Yasuda, T., Tsuduki, T., Kurisu, J. and Arimitsu, E., Improvement in adhesive resistance of tundish upper nozzle by modifying the inner bore profile, *Taikabutsu*, 2011,

Volume 63,No.2,pp.65-72(in Japanese).
45. Mizobe, A. and Ueki, M., Inner bore profile of the tundish nozzle minimizing alumina adhesion, *Refractories Applications and News*, 2011,Volume 16,No.2,pp.6-13.
46. Mizobe, A., Yasuda, T., Tsuduki, T., Kurisu, J. and Arimitsu, E., Determination of the optimal inner bore profile to tundish upper nozzle for improvement in adhesive resistance by computational fluid dynamics, *Proceedings of the 93rd Meeting of Technical Committee on Refractories for Casting, The Technical Association of Refractories, Japan*, 2011,pp.57-70(in Japanese).
47. Mizobe, A., Yasuda, T., Tsuduki, T., Kurisu, J., Oki, K.and Arimitsu, E., New tundish nozzle with the optimum bore profile,*Proc. UNITECR'11*, 2011,Paper No.2-A-1.
48. Spink, J., Carberry, M., Cassar, P., Mizobe, A., Yasuda, T. and Oki, K., Performance of a new tundish nozzle at operation in a steel plant, *Proc. UNITECR'11*, 2011, Paper No.2-A-2.
49. Mizobe, A., Tachikawa, K., Kurisu, J. and Ueki, M., Novel design of submerged-entry nozzle for steel continuous casting, AISTech-Iron and Steel Technology Conference Proceedings, 2017, pp.1989-2000.
50. Mizobe, A.,Kurisu, J., Furukawa, K., Tsuduki, T., Yamamoto, M., Oouchi, T. and Oki, K., Optimum quantity of gas blown into the bore of tundish upper nozzle, *Proc. UNITECR'13* 2013, pp.560-565.